Crack width numerical oriented-design approach for fibre reinforced concrete tunnel segments for TBM thrust loads

Alejandro Nogales-Arroyo[a,b], Albert de la Fuente[b]

[a]Smart Engineering Ltd., UPC Spin-Off, Jordi Girona 1-3, 08034 Barcelona, Spain

[b]Civil and Environmental Engineering Department, Universitat Politècnica de Catalunya (UPC), Jordi Girona 1-3, 08034 Barcelona, Spain

Abstract

Concentrated loads induced during the excavation stage by Tunnel Boring Machines (TBMs) is still a matter of discussion into the tunnelling construction field, this having a strong impact from both the technical (e.g., durability and service conditions) and the economic perspectives. Fiber reinforced concrete (FRC) has been gaining acceptance as a structural material for producing precast segments as this has proven to lead to various advantages respect to the traditional reinforced concrete, especially for improving the crack control during transient loading situations. In this sense, several experimental programs and numerical studies were previously carried out in which the different geometric and mechanical governing variables were analyzed and, from the results, valuable conclusions were derived. Nonetheless, there are still observed lacks and gaps related with the optimum reinforcement design (FRC strength class and/or amount of traditional steel bar reinforcement) which is often hindering the use of fibers as main reinforcement for concrete segments. The main purpose of the research consist in developing a parametric analysis related with the TBM-thrust effects on FRC segments by means of using a non-linear 3D FEM, previously calibrated with full-scale tests. The results are used to determine the range of FRC strength classes suitable for controlling the crack with during the TBM thrust phase. The results and conclusions are expected to be useful for tunnels designers when establishing the FRC mechanical requirements.

Keywords: Fibre reinforced concrete, TBM thrust, concentrated load, crack width, numerical simulation

1. Introduction

Over the last decades, the addition of fibres in concrete mixes has noticeable grown for structural purpose (Burgers et al., 2007; Chiaia et al., 2008; de la Fuente et al., 2015; di Prisco and Toniolo, 2000; di Prisco et al., 2009). Among the structural applications where FRC is used is tunnelling , precast tunnel segments are used to be suitable when using the Tunnel Boring Machines (TBM) excavation method (Blom, 2002; de Waal, 2000), even from the sustainability point of view (de la Fuente et al., 2017). The use of fibres in concrete mix has been proven as a potential solution and tunnel linings were made up with this material: "Barcelona Metro Line 9"(Burgers, 2006; de la Fuente et al., 2012; Gettu et al., 2004; Tiberti, 2004), "Monte Lirio Tunnel" in Panamá (Caratelli et al., 2011; de Rivaz et al., 2009); and the "Prague Metro Line" (Beňo and Hilar, 2013; Hilar et al., 2012) are examples, among others (in the *fib* Bulletin 83 (2017) more than 70 examples are gathered).

Experiences on tunnel design and researches have proven that in terms of loading and concrete cracking, the most demanding scenarios may not occur during the operational stage (Cavalaro et al., 2011; Sugimoto, 2006). Actions on tunnel construction can be classified in: (1) Primary loads due to soil-structure interactions and water pressure and (2) Secondary loads, which occurs during construction called transient phases, which include demoulding, storage, transportation, handling, placing and TMB jack's thrust.

Primary loads induce compressive forces combined with low shear forces and bending moments on the ring that can be resisted by the concrete matrix and a combination of fibre and conventional reinforcement

Nomenclature			
List of symbols		h	segment height
		P_{acc}	Accidental load
$A_{s,min}$	minimum reinforced area	P_{cr}	Cracking load
b	segment width	P_{spall}	Spalling cracking load
d	segment effective depth	P_{sp}	Splitting cracking load
$CMOD$	crack mouth opening displacement	w	crack opening in mm
E_{cm}	modulus of elasticity for concrete	w_s	crack opening for f_{Fts}
E_{ci}	tangent modulus of elasticity of concrete at a stress σ_i	w_{spall}	Spalling crack opening
E_{c1}	secant modulus from the origin to the peak compressive stress	w_{sp}	Spalling crack opening
f_{cm}	mean value of the cylindrical compressive concrete	w_t	crack opening when σ_j = 0
f_{ctm}	mean value of the tensile concrete strength	w_u	crack opening for f_{Ftu}
f_{Fts}	serviceability residual strength (post-cracking strength for serviceability crack opening)	ε_1	concrete strain for f_{ctm}
f_{Ftu}	ultimate residual strength (post-cracking strength for ultimate crack opening)	ε_c	concrete compression strain
$f_{R,j}$	value of the residual flexural strength corresponding to $CMOD = CMODj$	$\rho_{s,min}$	longitudinal reinforcement ratio
f_{yk}	yield strength of steel bar reinforcement	σ_c	concrete compression stress
G_F	fracture energy of concrete	σ_j	stress point for concrete tensile constitutive curve

in linings with large diameters (Liao et al., 2015; Plizzari and Tiberti, 2006; Tiberti et al., 2008); this situation is particularly frequent in case of predominance of soil homogeneity (e.g., no geologic faults existence), low probability and magnitude of seismic actions and/or no high internal water pressure (e.g. sewage-storage tunnels). However, in hydraulic or metro tunnels (less than 6.0 m diameter) mainly subjected to compression in service stage, it is during transient phases where tensile stresses appear either due to bending moments (during stacking, transport, handling and placing) or thrust phase where high concentrated loads lead to tensile stresses (splitting and spalling).

During excavation, high concentrated loads are exerted on the last placed ring by TBM jacks. The application of concentrated loads induces to a complex state of stresses, which both magnitude and distribution are difficult to be assessed due to the existence of a disturbance zone beneath the load transfer along a certain length called “D region”. This subject has been deeply studied and discussed by Leonhardt (Leonhardt and Mönnig, 1973) and Iyengar (1962) for transfer zones for pre-stressed structures. Compressive stresses trajectories in the region results in a tri-axial state of stresses where a principal tensile component of stresses (splitting stresses) acts orthogonally to the paths of compressions. In addition, on precast tunnel segments as a result of compatibility demand with respect to deformed cross section tensile stresses (spalling stresses) appear (de Waal, 2000).

These state of stresses and the bended shape of the elements lead to the use of conventional reinforcement with complex detailing, which may leave uncovered areas where spalling and splitting

stresses take place. Alternatively (or complimentary), FRC can deal with this matter due to the random distribution nature of the fibres within the whole segment. This FRC property is particularly interesting for covering those stresses derived from the TBM jacks' thrust and those due to the interaction of longitudinal joints, especially when seismic forces are expected to occur during the service live (Jamshidi et al., 2018a, 2018b).

It is worthwhile noticing that the magnitude of these forces depend on several factor such as surrounding ground type and friction forces between shield and soil, also the force exerted for each jack depends on the number of jacks used per segment, the loading plate area and its distribution (Slenders, 2002). Furthermore, some of the cracks may appear by imperfect placing of the segments or wrong TBM operation which generates load eccentricities and imperfect contact between adjacent rings (Burgers, 2006; Cavalaro et al., 2012).

Fibres of different materials (mainly metallic and synthetic) and geometries (length, thickness) are used in fibre reinforced concrete. While steel fibre reinforced concrete (SFRC) is the most used in tunnel lining constructions, there is a growing interest in synthetic fibres and several and extensive research has been developed on polypropylene fibres reinforced concrete (PFRC) in the last years (Conforti et al., 2016a, 2016b; Tiberti et al., 2015). Tests on specimens cast with PFRC, PC (plain concrete) and PFRC+RC (reinforced concrete) were carried out, combining loading situations (line and point load) and geometries (prismatic and plane specimens and tunnel segments).

Test results indicate that synthetic fibres can be a reinforcement solution for precast segments. Point load tests made on prismatic specimens (250x250x750 mm) with a total amount of 10kg/m^3 for evaluating the local splitting behaviour concluded that, taking PC as reference, synthetic fibres enhances the ductility and the bearing capacity up to +40%, the casting direction having a great influence on it. Tests on actual precast segments, using the same volume of fibres (10kg/m^3), demonstrated that polypropylene fibres can be used as flexural, splitting and minimum shear reinforcement. Furthermore, results pointed out that PFRC can be used as spalling reinforcement combined with conventional rebar and guarantees a better cracking control.

A remarkable advantage of synthetic reinforcement (either fibres or rebar) is in terms of corrosion resistance against aggressive environment especially for hydraulic tunnels (Caratelli et al., 2016). Experimental campaigns using glass fibre reinforced polymer (GFRP) rebar (Caratelli et al., 2016, 2017; Spagnuolo et al. 2017) concluded that there were no significant differences with steel rebar reinforcement on the flexural behaviour point of view and exhibited a better performance in terms of cracking reduction under concentrated loads. When a better flexural performance is required, GRFP rebar can be combined with SFRC (Meda et al., 2018).

Table 1 gathers several numerical and experimental programs related to FRC precast segments subjected to concentrated loads.

Elements	f_c [MPa]	Dimensions [mm]	Material	C_f [kg/m³]	Φ_f/λ_f	Tests	Load	Numerical Simulation	Ref.
PS (RP)	60	300 x 3000 x 1000 (panels)	RC SFRC	- 35 60	- 0.65/60 0.65/60 0.92/65	4	Centred jack	3D-FE (ANSYS)	Hemmy 2001
B (RP)	60	350 x 350 x 700	SFRC	35 60	0.65/60 0.92/60	12	Centred line and point load	3D-FE (ANSYS) and strut-tie models	Schnütgen and Erdem 2001
PS (MT)	50	900 x 520 x 175 (panels)	RC+SFRC SFRC	30 60	1.00/65	4	Centred and eccentric jack	3D-FE elastic model (ANSYS)	Gettu et al. 2004
PS (RP)	75-100	3150 x 1420 x 300	RC SFRC	- 60	- 1.00/50	5	Centred jack	3D-FE (ABAQUS) and strut-tie models	Sorelli and Toutlemonde 2005
PS (HT)	35	1840 x 1200 x 250	SFRC	40	0.75/80	1	Centred jack	None	de Rivaz et al. 2009
PS (RP)	60	2539 x 1400 x 350	PC SPFRC	- 30+1 40+1	- 0.75/80+ PP fibres	9	Centred Jack on cantilever supported segment	None	Pohn et al. 2009
PS (RT)	50	3400 x 1500 x 200	RC SFRC	- 40	- 0.35/85	2	Centred jack	None	Caratelli et al. 2011
PT (HT)	35	1840 x 1200 x 250	SFRC	40	0.35/85 0.60/50 0.75/40	3	Centred jack	Design with MC2010	Caratelli et al., 2012
PT (MT)	60	2570 x 1500 x 250	SFRC	40 50	0.75/80	15	Centred jack on uniformly and cantilevered supported segment	2D-FE (ATENA) and 3D-FE for the full-scale tests on precast segments	Beňo and Hilar 2013; Hilar et al., 2012
B (RP)	75-95	300 x 150 x 150	PC SFRC	- 40 60 80 60	- 0.75/80 0.90/65 0.71/85 0.55/55	96	Different loaded-area ratios with varying positions of the concentrated load	3D-FE (MSC-Marc)	Breitenbücher et al., 2014
PS (RP)	150-170	1000 x 500 x 100 (reduced scale)	UHPC UHSFRC	- 236	- 0.20/80	2	Centred TBM jack simulation	None	Abbas et al., 2014
B (RP)	50	250 x 250 x 750	PC PFRC	- 10	- 0.81/54	18	Centred line and point load	None	Tiberti et al., 2015
B (RP-MT)	40-50	(200-750) x 150 x 300	PC SFRC	- 40	0.75/60	32	Centred TBM jack simulation	None	Lin Liao et al., 2015b
PS (RP)	80	3000 x 1400 x 300	RC	-	-	31	Centred TBM jack simulations on uniformly and cantilevered supported segment	3D-FE (Diana TNO)	Meda et al., 2016
B (RP)	50-60	250 x 250 x 750	SFRC	10	0.66/55 0.8/75	6	Centred line load	None	Tiberti et al., 2015
PS (RP)	50-60	1000 x 750 x 150 (reduced scale)	PFRC PC RC+PFRC	10 - 10	0.80/67	8	Centred line and point load	None	Conforti et al., 2016a
PS (RP-MT)	60	1920 x 1200 x 250	RC PFRC RC+PFRC	- 10 10	0.81/67	3	Centred TBM jack simulation	None	Conforti et al., 2016b
PS (RP)	50	4150 x 1483 x 250	GFRP	-	-	2	Centred TBM jack simulation	None	Caratelli et al., 2016

PS (RP)	60	3000 x 1400 x 300	GFRP+ SFRC SFRC	40	0.75/60	2	Centred TBM jack simulation	None	Meda et al., 2018
PS (RP-MT)	40	3020 x 1420 x 300	RC RC+PRFC	10	0.81/55	2	Centred TBM jack simulation	None	Conforti et al., 2019

Table 1 – Previous research focused on FRC elements subjected to concentrated loads

PS: precast concrete segment;	MT: metro tunnel;	RC: reinforced concrete	C_f: amount of fibres
B: concrete block;	HT: hydraulic tunnel;	SFRC: steel fibre reinforced concrete	Φ_f: diameter of the fibre
RP: research project;	RT: road tunnel	PC: plain concrete;	λ_f: slenderness ratio of the fibre
UHPSFRC: Ultra high performance steel fibre reinforced concrete	UHPC: Ultra high performance reinforced concrete	PFRC: Polypropylene fibre reinforced concrete	GFRP: Glass fiber reinforced polymer rebar

Comprehensive parametric studies have been done in these programs. As can be seen in Table 1, steel fibres amounts ranged from 35 to 80 kg/m^3 and 10 kg/m^3 in case of synthetic fibres are commonly used. Abbas et al. (2014) tested a segment with 236 kg/m^3 of micro steel fibres in order to evaluate the structural benefits of using ultra-high performance steel fibre reinforced concrete (UHPSFRC). Fibre orientation influence on FRC performance was considered in Sorelli and Toutlemonde (2005), Breitenbücher et al. (2014) and Tiberti et al.(2015). Most of the analysed tests applied a centred load, either line or point load, except for Gettu et al. (2004) and Breitenbücher et al. (2014) which also studied the influence of eccentric loads. In order to simulate an imperfect support between adjacent rings, several researchers have set tests with a cantilever configuration support (Beňo and Hilar 2013; Hilar et al., 2012; Meda et al., 2016; Pohn et al., 2009). Furthermore, the loading area is a topic of concern, Breitenbücher et al. (2014) and Conforti et. al (2016a) analysed the influence of the contact area on the response.

Numerical analysis were made using finite element (FE) packages. Those most commonly used for simulating the TBM thrust jack were: ANSYS (Swanson Analysis Systems, 2013), ATENA (Cervenka et al., 2013), ABAQUS (Dassault systems Simulia, 2012), DIANA (Manie and Kikstra, 2008) and MSC-Marc (MSC Software Corporation, 2008). These FE softwares are capable of reproducing the nonlinear response due to cracking of concrete and FRC after reaching tensile strength. The post-cracking response modelling can be done in several ways: smeared crack, discrete cracking and damaged models. The numerical analysis results compared to those obtained in experimental campaigns showed that the response of the model were in good agreement with the nonlinear behaviour and cracking of the tested FRC segments.

Furthermore, it must be highlighted that several guidelines have included FRC design recommendations such as DBV (2001), RILEM TC 162-TDF (2003), CNR-DT 204/2006 (2007), EHE-08 (2008), *fib* Model Code (2010) and ACI 544 (2014) and specific documents have been published recently for supporting the design of precast tunnel segments (*fib* Bulletin 83 (2017) and ACI 544.7R-16 (2016)) to the practitioners.

In regard to thrust phase, despite being a temporary stage, can influence the design of precast tunnel segments. This phase is the most frequent source of cracking cause during tunnel construction and lifetime (Sugimoto, 2006). The thrust phase can jeopardize costs, structural durability and the serviceability of the tunnel: the corrosion arising from cracks in aggressive environments due to carbonization and chloride ions undermine reinforcement and in case of sewage and water supply tunnels a completely watertightness is required.

The response of the segment under concentrated loads is difficult to evaluate and analyse, in particular for FRC when some cracking is permitted. The evaluation of fibres benefits under concentrated loads in a design process can be done experimentally, either by local experimental tests (splitting tests) or global experimental tests (full-scale tests), or by means of a non-linear numerical analyses of FRC tunnel segments (*fib* Bulletin 83, 2017). Knowing how the segment subjected to concentrated loads performs is of great interest since compromises designing (segment geometry, amount and reinforcement distribution) and therefore costs.

Despite many experimental and numerical research can be found in the literature, most of them are focused on studying the benefits of using fibres as partial (or total) reinforcement for splitting stresses under concentrated loads. Spalling phenomena has barely been studied (Meda et al. 2016; Conforti et al., 2016a, 2016b) although these is the most common crack pattern reported for thrust phase (Sugimoto, 2006). FRC results are commonly compared with PC or RC and a lack of research is found when comparing between FRC classes, which has been introduced in the *fib* MC-2010 in order to classify the post cracking strengths of FRC. The effect of using different FRC and its mechanical response, cracking and ultimate load has not been yet studied and many questions arise when dealing with precast FRC segments, how affect using different FRC classes and until where improving the FRC strength (higher FRC class) affects the cracking and structural response of the whole segment.

The aim of this paper is to evaluate the structural performance of TBM constructed tunnels with FRC precast segmental linings under thrust jack forces. The main goal consists in analysing the effects of precast segments cast with different classes of FRC according to *fib* MC-2010 and provide a range of classes that can be the more advantageous reinforcement solution for future tunnel designing. The FRC results are to be compared also with PC, RC and hybrid reinforcement (FRC+RC). A comprehensive non-linear numerical simulation campaign was carried out using a finite element software package ABAQUS (Dassault systems Simulia, 2012); the model being previously calibrated by using results derived from other experimental programs. Both the results and conclusions achieved are of interest in terms of structural and economic optimization in those cases for which the TBM thrust is the design governing phase.

2. Numerical modelling of FRC

According to *fib* Bulletin 83 (2017), the design of FRC tunnel segments subjected to concentrated loads can be carried out by non-linear FE analysis. Regarding the modelling of the FRC mechanical response, according to *fib* MC-2010, the FRC strength class can be ranged by the characteristic values of the flexural

residual strength (f_{Rk}) obtained from the three point bending test on notched-beams according to EN 14651:2005. Two parameters are used for classifying: f_{R1k} that represents the residual strength for a crack mouth opening displacement (CMOD) of 0.5 mm and a letter (a, b, c, d or e) that represents the f_{R3k}/f_{R1k} ratio, where f_{R3k} stands for a COMD of 2.5 mm.

To establish the compressive stress-strain (σ-ε) and tensile stress-crack opening (σ-w) constitutive relationships from *fib* MC-2010 are used, see Figure 1. Mean values of each of the involved mechanical variables are considered for the numerical simulations.

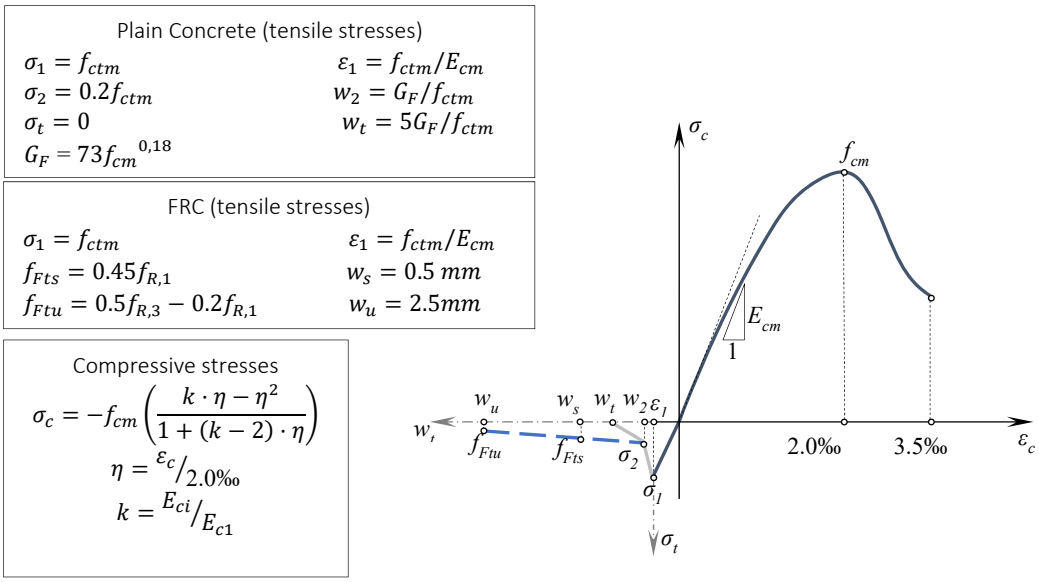

Figure 1 – Constitutive equations for concrete; σ-ε for compression and σ-w for tensile

With the purpose of implementing the FRC post-cracking response in the software, the Concrete Damage Plasticity (CDP) model (Dassault systems Simulia, 2012) available in the software is used. The CDP model is a continuum, smeared crack, plasticity-based, damage model for concrete. In smeared crack models the damage zone coincides with the element dimensions. The model assumes that the main two failure mechanisms are tensile cracking and compressive crushing of the concrete material. In order to reproduce the concrete behaviour the input data required are uniaxial σ-ε curves for compression and tension. It is worth noticing that to overcome mesh dependence the σ-w tensile curve is used instead. In this regard, the σ-w tensile and σ-ε compression curves proposed by the *fib* MC-2010 are used for the analysis, the characteristic length (L_{ch}), to turn crack opening into strain, implemented by default by the software is the size of the element. The CDP parameters adopted in all the simulations of this research work are the default ones proposed in ABAQUS User's Manual (2012) for plain concrete.

3. Experimental model validation

3.1. Small-scale blocks (Schnütgen and Erdem, 2001)

Small-scale experimental tests carried out by Schnütgen and Erdem (2001) which consisted in SFRC anchor blocks subjected to concentrated loads oriented to assess the response against splitting (Dupont et al., 2001) is taken as reference for calibrating the model. This campaign has previously been used for other

model validations (Burgers, 2006). To this end, twelve blocks (350 x 350 mm in cross-section, 700 mm high) cast with three different SFRC mixes and subjected to line loads (Figure 2a). LVDT transducers were placed on the frontal face, perpendicular to the load, to measure displacements (horizontal) produced by splitting stresses. 35 kg/m^3 (SFRC-A) and 60 kg/m^3 (SFRC-B) of hooked-end steel fibres (0.75 mm in diameter and 60 mm in length) were used for produce the SFRC mixes. The average compressive concrete strength (f_{cm}) was 58.2 N/mm^2 and 50.2 N/mm^2 for SFRC-A and SFRC-B, respectively. The average equivalent flexural residual strengths (f_{eqm}) measured according the NBN-B-15-238:1992 were 5.41 N/mm^2 ($f_{eqm,1}$) and 4.81 N/mm^2 ($f_{eqm,3}$) for SFRC-A and 6.49 N/mm^2 and 5.96 N/mm^2 for SFRC-B.

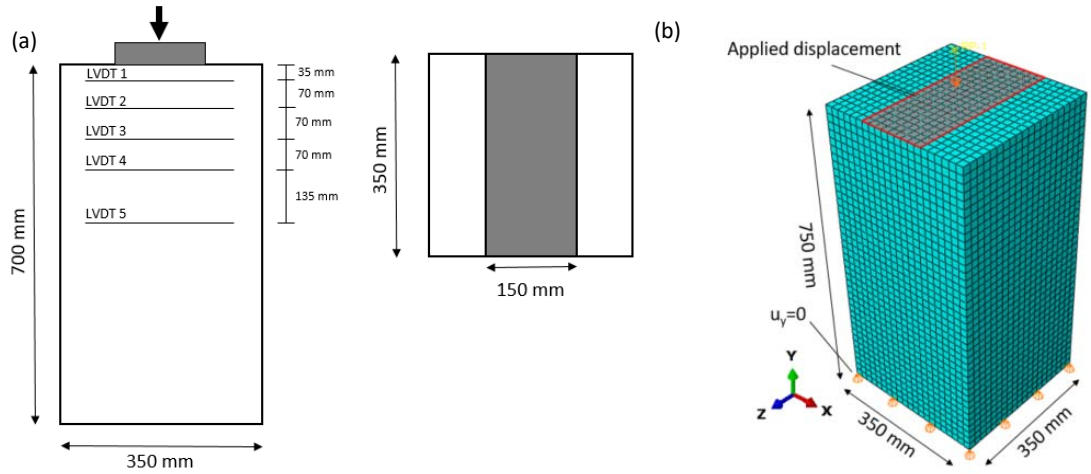

Figure 2 – Splitting Line Load test (a) Lab test configuration and (b) FE model meshed considered

A non-linear 3D model was implemented (Figure 2b) to simulate both the geometry and loading conditions presented in Figure 2a. The mesh consists of 8-noded solid linear hexahedral elements (C3D8R) used for modelling concrete, this leading to an amount of 16,800 elements. Vertical displacement is restricted (u_y=0) at the bottom face and the load is applied by displacement control, in order to guarantee a better convergence, on a 350 x 150 mm surface on the top according to the test configuration (Figure 2a).

Figure 3a and 3b present the stress pattern on the block for a load $P = P_{sp}$ (Splitting load) /2 (1030 kN), where S11 stands for stress in x direction (MPa). In Figure 3c for the same load level, together with the numerical model stress data, obtained from integration points throught a straigth vertical line in the mid section (Figure 3b), is presented the elastic solution according to the abacus for concentrated loads proposed by Iyengar (1962), later corroborated Leonhardt and Mönnig (1973). It can be noticed that the model reproduces accurately the behaviour at this pre-cracked regime. The splitting load measured averaged 2500 kN for the four specimens tested and it resulted to be 17.6% lower according to the numerical model (2060 kN).

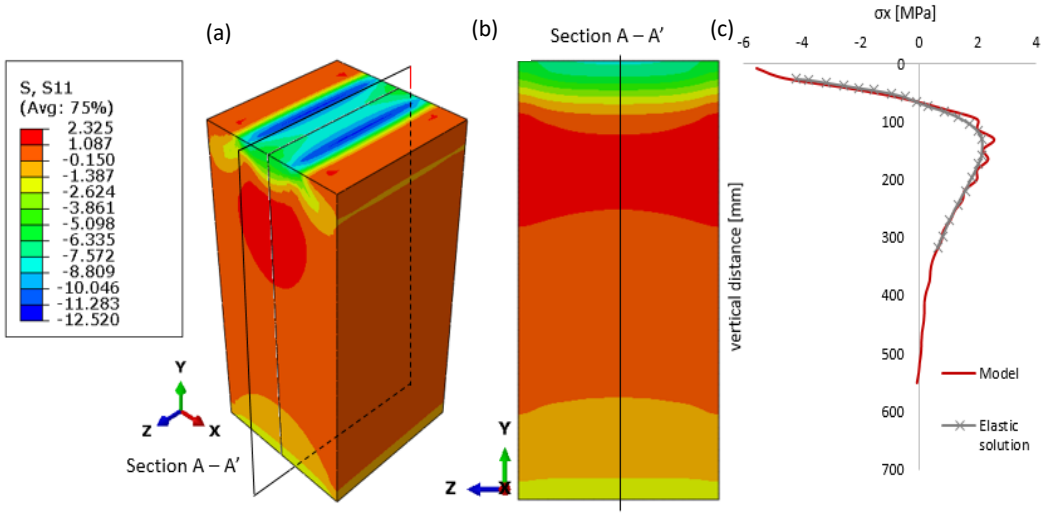

Figure 3 – Stress state in N/mm² for P=1030 kN (a) full specimen (b) mid-section (c) along straight line

Figure 4 and 5 presents both the experimental and numerical results for the SFRC-A and SFRC-B respectively, in terms of load-horizontal displacement at a distance of 175 mm from the top (LVDT 3) where the maximum tensile stresses appear due to splitting (see Figure 3c).

The specimen with SFRC-A (Figure 5a) presented maximum experimental loads of 3,200 kN (1A) and 2,870 kN (2A) while the numerical results reached a maximum load of 2,880 kN. SFRC-B specimens (Figure 5) reached a maximum load up to 2,830 kN (1B) and 2,650 kN (2B), whereas the numerical model presented a magnitude of 2,815 kN.

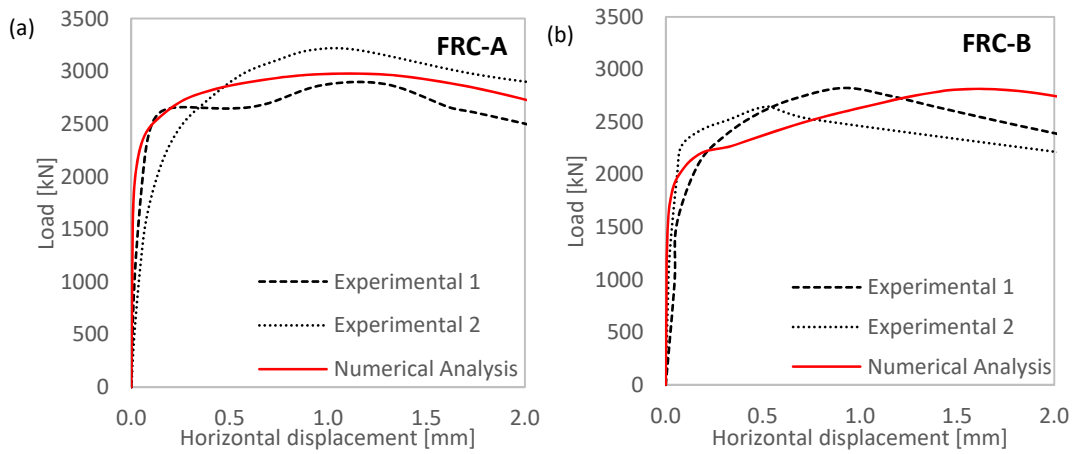

Figure 4 – Experimental and numerical load-horizontal displacement curves –(a) Concrete A and (b) Concrete B

Finally, Figure 5 includes the crack pattern reported and the one obtained numerically. The first crack is vertical and appears at the center of the specimen and progressively grows downwards while another cracks appear in the region under the loading pad, these growing until the merge with the former.

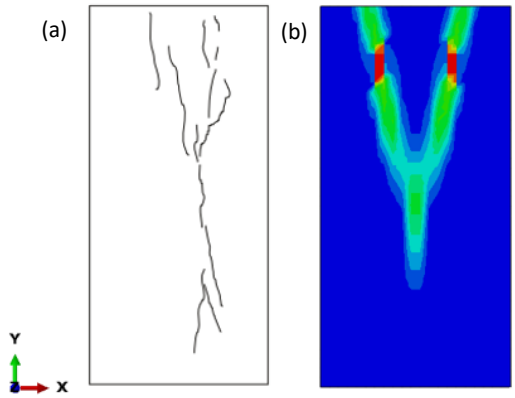

Figure 5 – Crack pattern (a) experimental test (b) model

Thus, according to the results presented in Figures 4-5, it can be remarked that the model can reproduce properly the mechanical response of SFRC short blocks subjected to concentrated line loads that generate splitting stresses and capture the resistant mechanism up to failure.

3.2. Full-scale non-curved segments (Conforti et al., 2016a)

Experimental program carried out by Conforti et al. (2016a) to evaluate the contribution of polypropylene fibres in controlling both the splitting and spalling phenomena in tunnel segments is the second experimental campaign used for the model calibration. Test were done on 8 non-curved 150 x 1000 mm in cross-section and 750 mm high specimens, combining different reinforcement configurations: PFRC and RC. Loads were applied through pads considering centred loads with different widths of loading area (100 and 150 mm) on full-supported segments. Figure 6a presents the test set up, reinforcement configuration and the position of the measure devices for detecting and measuring the crack opening: potentiometric transducers (PTs) for splitting and linear differential transformers (LVDTs) for spalling cracks. 150 mm width loading area tests are used to compare. The segment were cast using three different reinforcement and concrete configurations: (1) PFRC with 10 kg/m^3 fibre amount, 48.3 N/mm^2 f_{cm} and 2.4 and 3.6 N/mm^2 for f_{R1m} and f_{R3m} respectively, according to EN-14651:2005, (2) same PFRC mix combining fibre and conventional reinforcement: top and bottom 4Ø8 chord were placed at a 120 mm depth and two-leg Ø6 stirrups at a distance of 150 mm in each chord with 552 N/mm^2 yield stress for steel rebar (RC+PFRC) and (3) PC with 57.2 N/mm^{2}compressive strength.

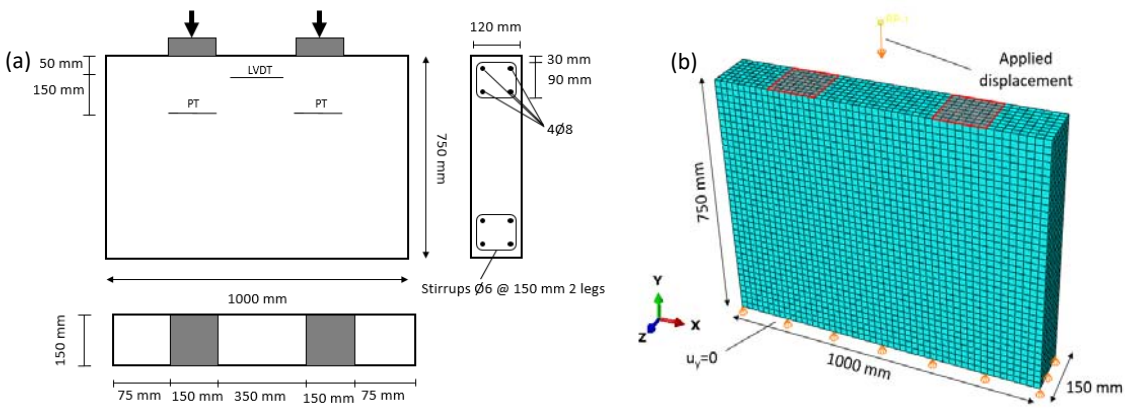

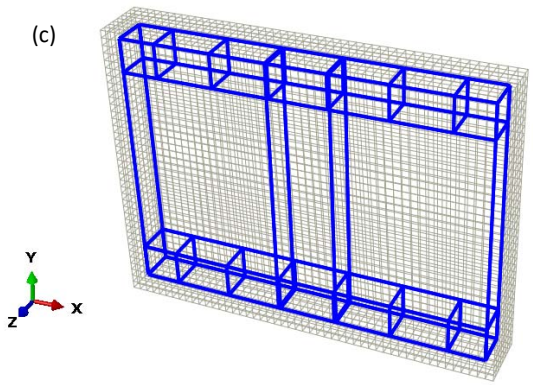

Figure 6 – Segment test (a) Test set up (b) meshed model and boundary conditions (c) meshed model reinforcement

The non-linear model is set by 20,000 elements, the concrete is modelled using C3D8R hexahedral elements and the steel rebars are reproduced with 2-noded 3D linear truss elements (T3D2) embedded into the solid elements. The embedded region constraint method available in ABAQUS is used to join the reinforcement with concrete. In Figure 6b is shown the meshed model and the boundary conditions: displacement is restricted at the bottom face (u_y=0). For the sake of convergence, the load is applied by displacement control on a top 150 x 150 mm surface. In Figure 6c the meshed model showing the reinforcement distribution is presented.

The cracking loads due to spalling (P_{spall}) and splitting stresses (P_{sp}) as well as maximum load (P_{max}) are presented in Table 2. Besides, the maximum crack opening for spalling (w_{spall}) and splitting (w_{sp}) obtained experimentally and numerically are gathered. In the numerical model, spalling cracks, which appear between the load pads, and splitting cracks, which are produced under the load pads, were measured as the relative separation between two adjacent nodes in the element in which the plastic strain is detected.

Type	P_{spall} [kN]	w_{spall} [mm]	P_{sp} [kN]	w_{sp} [mm]	P_{max} [kN]
PC	725 (*-3.1%*)	1.60 (7.0%)	1901 (-13.2%)	-	1901 (-13.2%)
PFRC	692 (*-10.2%*)	0.26 (7.1%)	1476 (8.0%)	0.84 (6.7%)	1995 (-0.7%)
PFRC+RC	695 (*-32.4%*)	0.36 (12.5%)	1610 (-1.9%)	0.62 (13.9%)	1895 (-2.1%)

Table 2 – Numerical loads and crack opening (relative error respect to the experimental results, negative values indicate that the numerical model overestimates the experimental result)

The results reported in Table 2 confirm that the model tends to overestimate load capacities (from 0.7% to a maximum of 32.4%) whilst the crack widths resulted to be overestimated (with a maximum relative difference of 13.9%). In view of this, it can be remarked that the agreement between experimental and numerical results is acceptable from designing perspective. In this sense, it should be remarked that damage level of the left side of Figure 7a, particularly the splitting area, is more severe than that observed in the right side, which is aligned with that obtained in the numerical simulation. This asymmetrical response might be due to a non-desired (and technically unavoidable) imperfections at the support contact area and/or slight deviations of the load position. It should be also highlighted that the damage pattern

depicted in Figure 7a corresponds to a post-failure loading regime, which is difficult to simulate and out of the scope of these type of simulations.

Crack pattern at failure for PFRC are shown in Figure 7, as it can be seen spalling and splitting cracks, are well captured in the model. The results presented in this section show that the model can reproduce the global response of the segment when induced by concentrated loads, reproducing splitting and spalling stresses properly.

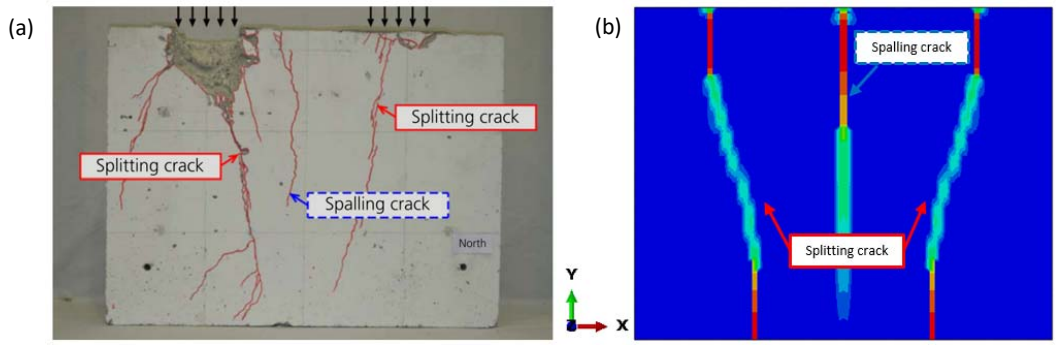

Figure 7 – Crack pattern (a) experimental test (b) model

3.3. Full scale curved segment (Conforti et al., 2016b)

In order to evaluate the model with a curved segment subjected to concentrated loads another experimental research work carried out by Conforti et al. (2016b) was used. Again, the contribution of polypropylene fibres in controlling the spalling is evaluated. To this end, a test is performed on a curved segment of 1810 mm length (internal diameter of 3200 mm), 1200 mm height and 250 thick subjected to concentrated loads by means of two loading shoes (500 x 250 mm). The segment is cast with 10 kg/m^3 polypropylene fibres, 49.9 N/mm^2 f_{cm} and 2.97 and 4.61 N/mm^2 for f_{R1m} and f_{R3m} respectively, according to EN-14651:2005. Figure 8a presents the test configuration, geometry and the position of the measure devices for detecting and measuring the crack opening: potentiometric transducers (PTs) for segment shortening in vertical direction and linear differential transformers (LVDTs) for spalling cracks.

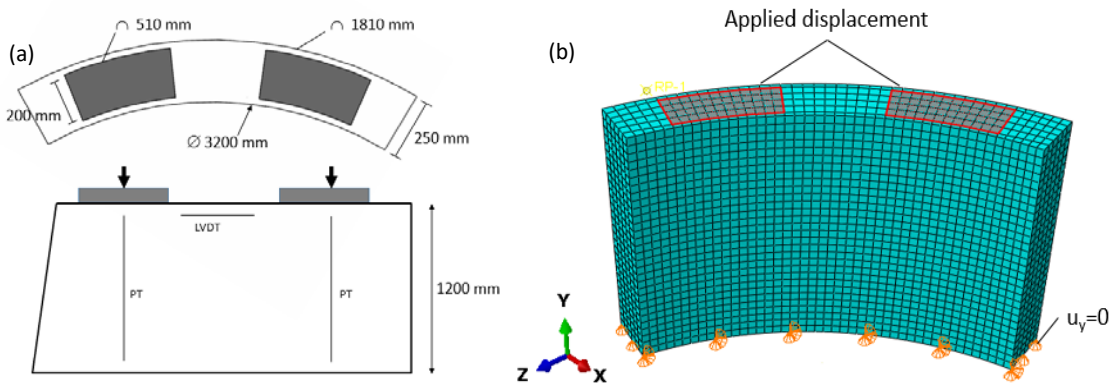

Figure 8 – Segment test (a) Test set up (b) meshed model and boundary conditions

8,100 C3D8R hexahedral elements were used for modelling concrete. For the sake of simplicity and to obtain a regular mesh, the original geometry was changed and a regular geometry is used. This simplification has negligible influence on local behaviour which do not affect the results of splitting and spalling phenomena that are produced under the loading zone and between pads. In order to reproduce the experimental test conditions the only boundary conditions adopted is zero displacement at the segment bottom layer (u_y=0). The load is apply by displacement control on top surfaces, representing the shoes, in order to guarantee a proper convergence (Figure 9b).

In Figure 9a the load - vertical displacement is presented. It is worth noticing that the model performs similarly to the experimental one up to 1200 kN, the P_{spall} is 995 kN and 979 kN for both experimental and numerical (-1.60%) and the P_{sp} was 1600 kN in the experimental test whereas 1585 kN is registered in the model (-0.93%). In the actual project the operational load (P_{nom}) and the accidental load (P_{acc}) were 785 kN and 1130 kN respectively. The spalling crack is measured and depicted in Figure 9b. In the numerical model, spalling cracks, which appear between the load pads (Figure 10b), was measured as the relative separation between two adjacent nodes in the element in which the plastic strain is detected. The spalling crack at P_{acc} (1130 kN) is 0.05 mm and the registered in the numerical model is 0.034 mm. Figure 10 shows the crack pattern obtained in the experimental and numerical test.

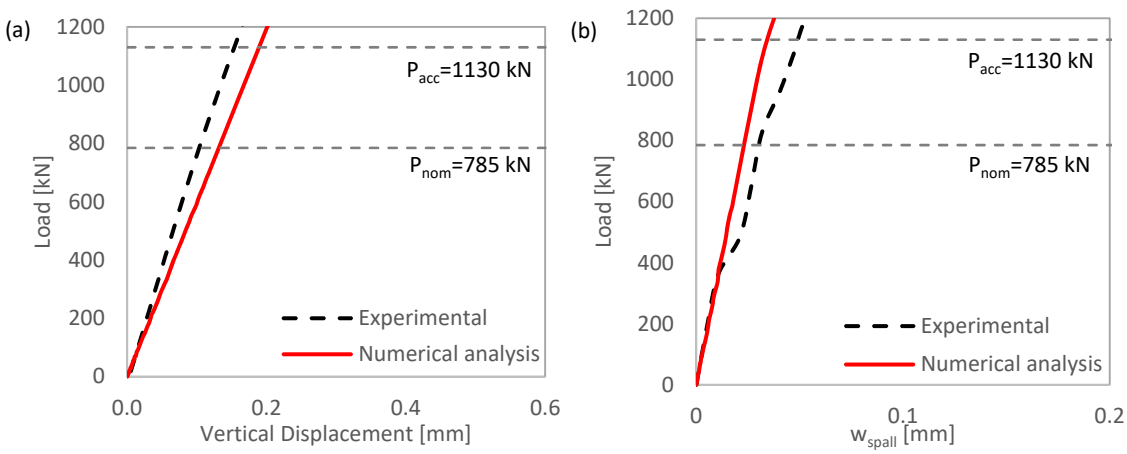

Figure 9 – Experimental and Numerical comparison (a) Load-vertical displacement (b) Load-spalling crack opening

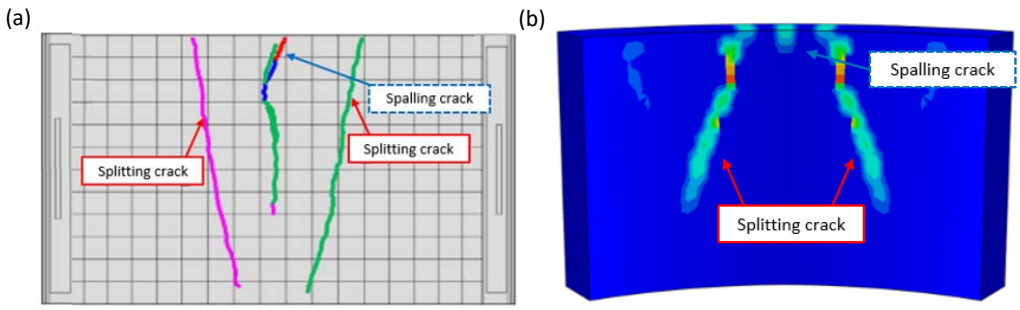

Figure 10 – Crack pattern (a) experimental test (b) model

According to the results presented in Figures 9-10, it can be remarked that the model can reproduce properly the mechanical response of FRC curved tunnel segment and the crack pattern that is developed when are subjected to concentrated loads.

4. Numerical parametric study on FRC and RC/FRC segments subjected to concentrated loads

4.1. Segment geometry

The segment geometry and jack configuration are both taken from precast segment of an actual metro tunnel lining under construction. Since there are no point load tests conducted on the actual segment the results presented in Section 3 allow to validate FE model for precast segments under concentrated loads. The segment has 4075 mm inner radius, is 1500 mm width (tunnelling direction), 350mm thick and 4010 mm of arc-length (see Figure 11). The Japanese configuration (Slenders, 2002) has been used for the TBM jacks distribution, this consisting in four 222 x 500 mm rectangular pads placed at 42 mm from the internal edge.

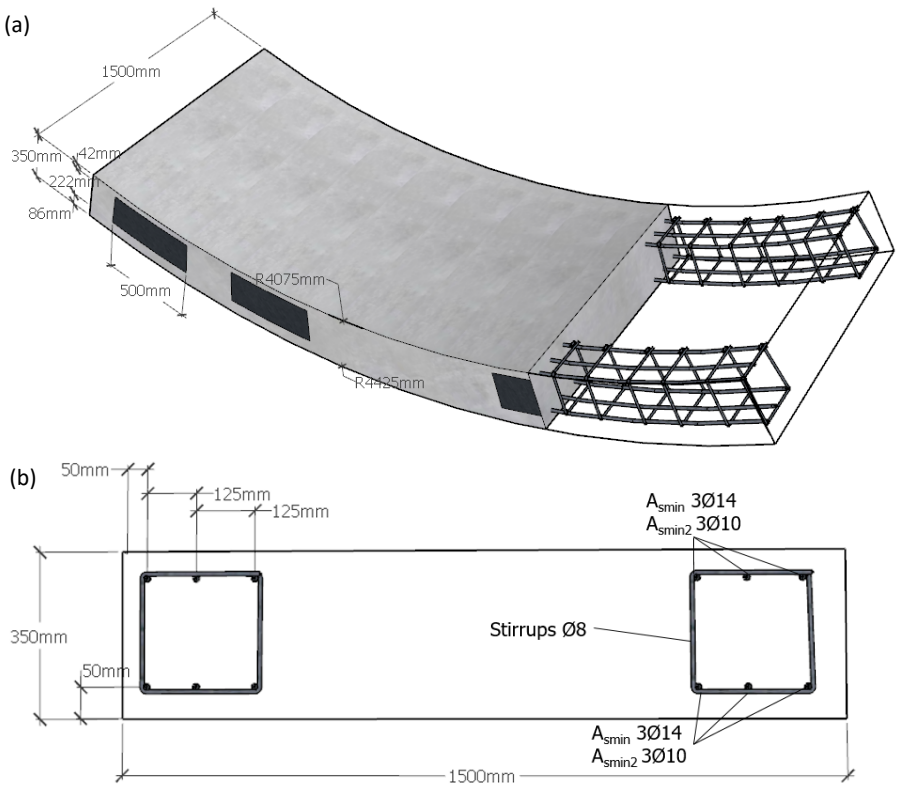

Figure 11 – Geometrical properties of the segment (a) general layout and (b) cross section and reinforcement distribution

4.2. Materials

A C50/60 concrete has been used for the production of these segments; thus, according to the *fib* MC-2010, the values f_{ctm} = 4.07 N/mm^2, f_{cm} 58 N/mm^2 and E_{cm} = 32900 were assumed. The FRC strength classes 1, 3 and 5 (related to f_{R1k}) with f_{R3k}/f_{R1k} ratios a, b, c, d and e (see *fib* MC-2010) were considered for simulating different FRC performances (see Figure 12), these resulting in a total of 16 different concretes (15 FRC + 1 PC). The commonly accepted ratio f_{Rk}/f_{Rm} = 0.7 was used to estimate f_{Rm}. Thus, mean values of

the crack widths (w_m) were obtained from the numerical simulations. For design checks, if required, the characteristic value of w (w_k) could be estimated as $w_k = \beta \cdot w_m$, β being 1.7.

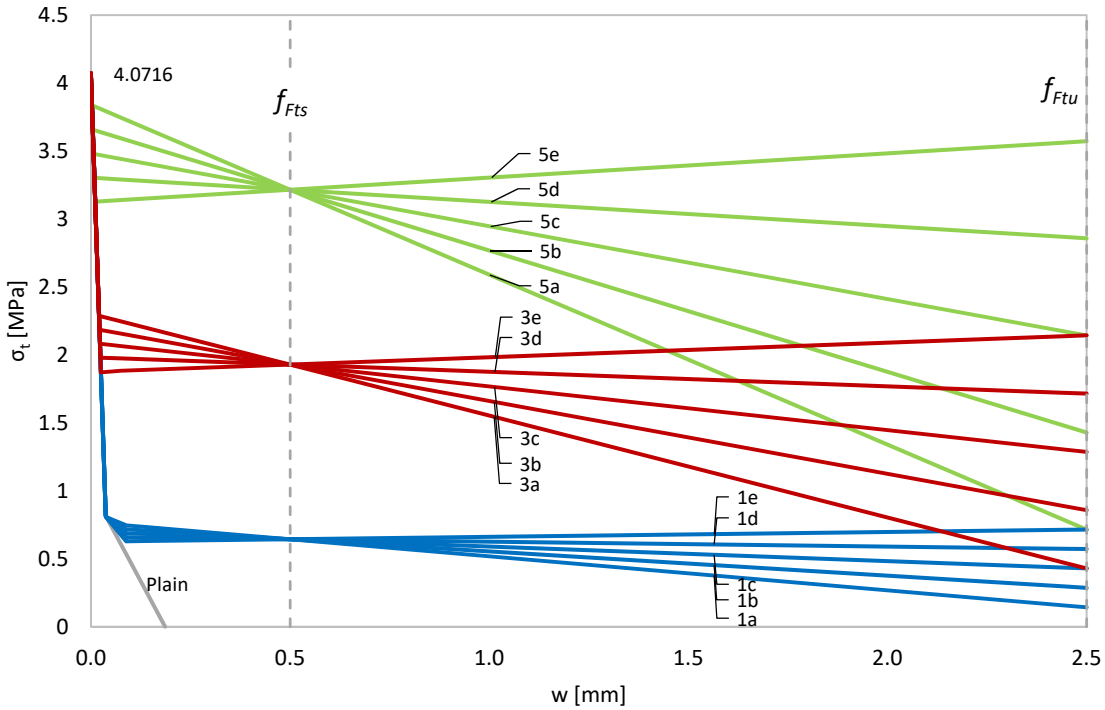

Figure 12 – Tensile constitutive equations of concrete mixes

Furthermore, aiming at optimising the reinforcement configuration, the hybrid reinforcement (RC+FRC) is also considered. Figure 11 b shows the segment rebar configuration, this being composed by two chords made by 2x3Ø14 curved rebars with Ø8@200mm stirrups, with a clear cover of 50mm. This amount (per face) corresponds to the minimum amount ($A_{s,min}$) required by *fib* MC-2010 to guarantee the ductile response. This minimum amount is computed with Equation 1, *b* being the segment width (1500 mm), *d* the effective depth and f_{yk} = 500 MPa is the characteristic value of the steel yielding stress. The reinforcement ratio, ρ_s, is calculated as Equation 2, where *h* corresponds to the segment height. It must be highlighted that the contribution of the fibres has been disregarded when computing the minimum amount of steel rebars, Liao (Liao et al., 2015a, 2016) proposed a method for assessing the minimum reinforcement of hybrid segments. Additionally, a ratio of $\rho_{s,min}/2$ (2x3Ø10 each face) has also been included into the analysis.

$$A_{s,min} = 0.26 \cdot b \cdot d \cdot {f_{ctm}}/{f_{yk}} \qquad (1)$$

$$\rho_{s,min} = {A_{s,min}}/{b \cdot h} \qquad (2)$$

4.3. Model description

Figure 11 shows a general view of the mesh and boundary conditions of the segment model. Simplifications must be taken in order to guarantee a robust model with a non-dependent mesh able to reduce computational calculation time while giving accurate results. Only a single segment is modelled, the

interactions with the surrounding segments at longitudinal and radial joints are not taken into account, these interactions has negligible influence on local behaviour which do not affect the results of splitting and spalling phenomena that are produced under the loading zone and between pads, besides this assumption helps to avoid convergence problems and reduce computational time. For the same reason, in spite of setting a regular mesh, bolt and gasket holes are not modelled.

In order to apply concentrated loads, thrust loads can be modelled as contact between packers and segment, which can produce convergence problems. Instead, using a quasi-static solver, the load is applied by means of displacement control loading on top surfaces representing the bearing pads.

Boundary conditions applied on the segment are: (1) vertical displacement restricted (u_y=0) at the bottom, (2) vertical displacement on top 222 x 500 mm surfaces (see Figure 13).

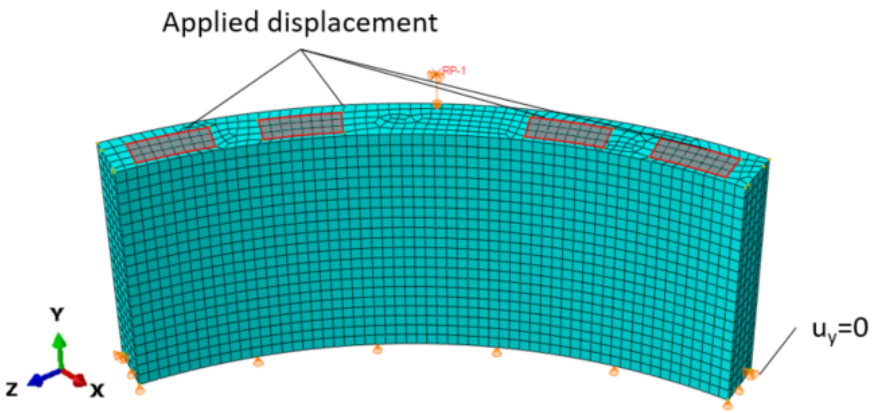

Figure 13 – Meshed model and boundary conditions

The concrete is modelled using C3D8R hexahedral solid elements and the 2 nodes 3D linear truss elements T3D2 are chosen for reinforcement, embedded constraint is used for join linear and solid elements. The embedded constraint creates a perfect bond between concrete and steel. After a mesh convergence analysis using the explicit solver implemented in ABAQUS (quasi-static analysis), a 70 mm size element has resulted to be suitable in terms of computational costs and preciseness.

5. Numerical results and discussion

5.1. Centred thrust

The first crack is due to spalling stresses between the two inner load pads, this cracking load (P_{cr} = P_{spall}) is 1975 kN for each pad and this is taken as reference load for all cases of analysis since this is independent of the reinforcement configuration. The so called nominal load (P_{nom}) is the TBM work load, which is 480 kN for each pad in the actual project, and should be lower than the cracking load so that the integrity of the segment can be guaranteed. Within the context of this analysis, the ratio P_{cr}/P_{nom} has been established to be 1.0. In this sense, although P_{nom} is far below P_{cr}, it must be remarked that the same ring geometry and segment configuration could be used in other tunnels with more demanding TBM thrust conditions. Figure 12 shows the non-dimensional load ($P/P_{spalling}$) - axial displacement of the jack (δ). The *c* class has

been taken as reference ($0.9 \leq f_{R3k}/f_{R1k} < 1.1$) since, according to the *fib* bulletin 83, this allows guaranteeing that FRC segments to show a ductile response in case of cracking due to bending.

As it can be noticed in Figure 14, P_{spall} is far from the maximum bearing load, which ranges between 2.5 and 3.2 times depending on the fibre content. The accidental thrust (P_{acc}) depends on the TBM type and equipment installed; the ratio P_{acc}/P_{nom} use to range between 1.2 up to 2.0. The higher ratio ($P_{acc} = 2 \cdot P_{nom}$ = 3950 kN) has been considered in this analysis. The P/P_{spall} - δ resulted to be identical for all mixes up to $P/P_{spall} = 2.5$.

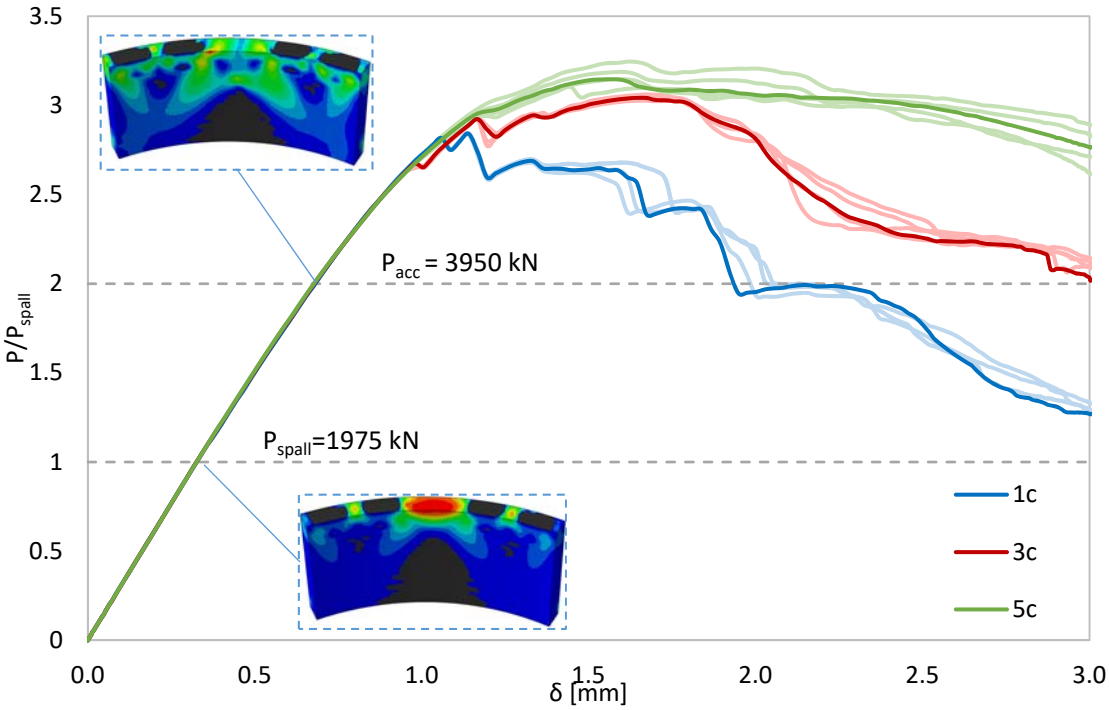

Figure 14 – Non-dimensional load-displacement curve for FRC. Stress pattern for P_{spall} and P_{acc}

The deformed shape of the segment is depicted for P_{spall} for stresses in tangential direction (S22 in MPa) and the crack pattern (plastic strain in tangential direction) in Figure 15a and 15b respectively, as aforementioned the region between the inner thrust pads is where spalling stresses concentrate and once it exceeds the tensile strength of the concrete the crack appears. In this case, the concrete is able to reach the tensile strength (4.07 MPa) because the tangential direction is the only prevented from displacement (symmetry) while the radial and the axial are both free, all the stress is born in tangential direction.

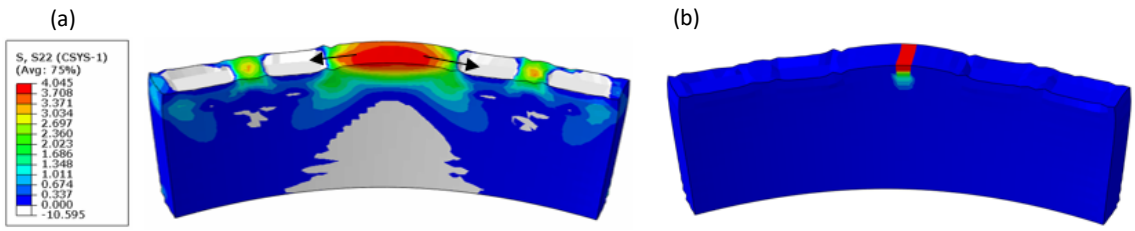

Figure 15 – Segment deformed shape for P_{spall} (a) Tangential tensile stresses (b) plastic strain - crack pattern

Figure 16 gathers the (P/P_{spall}) - spalling crack opening (w_{spall}). The crack opening is based on the assumption that only one spalling crack occurs, which is measured as the tangential relative separation between two adjacent nodes (separated 60 mm) of the element for which the plastic strain is first detected. This means that the concrete tensile strength has been exceeded and concrete cracked thereof (Burgers, 2006; Tiberti, 2004).

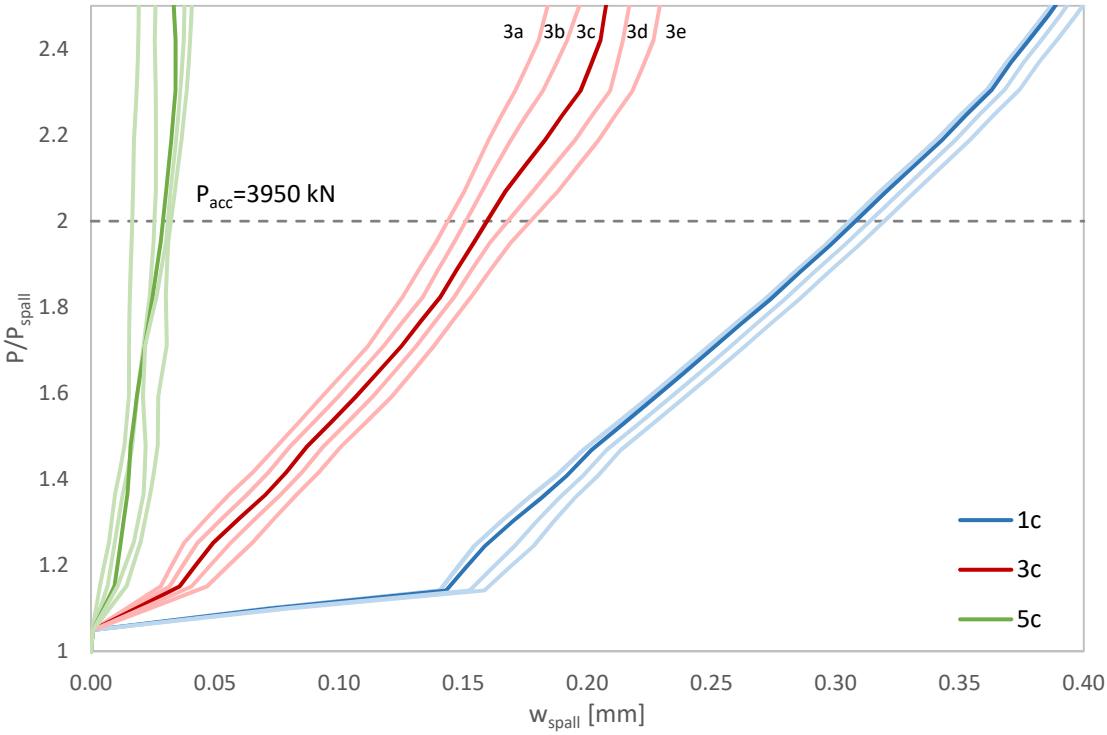

Figure 16 – Non-dimensional load – spalling crack opening

The results presented in Figure 16 allows confirming that f_{R1} has a great influence in cracking control while the strength ratios f_{R3}/f_{R1} do not play a significant role (once f_{R1} is defined). This was expectable since f_{R3} is a strength parameter associated to a 2.5 mm crack width and, therefore, beyond the range accepted for service conditions ($w \leq 0.5$ mm). In this regard, the maximum w_{spall} detected for P_{acc} are 0.38, 0.30, 0.16, and 0.03 mm for Plain, 1c, 3c, and 5c, respectively.

In view of these results, the 3c FRC class can be the more advantageous reinforcement solution for this segment from both economic and technical points of view, as: (1) a crack with of 0.16 mm is acceptable for an exceptional load (unless very strict durability and waterproof requirements are established) and (2) a near 50% of crack width reduction respect to the 1c FRC class represents a great efficiency of the reinforcement for a low increment of the amount fibres necessary to reach the 3c FRC strength class. In view of this, the *c* type is fixed throughout the remaining analysis. This is aligned with the preference of the *fib* Bulletin 83 towards this FRC performance class for tunnel segments.

Splitting cracks under the inner thrust pads are detected for P_{sp} = 2173 kN ($1.1P_{nom}$). Because of the tri-axial state of stresses the cracking is produced before reaching the tensile strength in any direction. In Figure 17 a S11 stands for stress in radial direction (MPa). In this case, the splitting crack opening (w_{sp}) is calculated

as the radial relative displacement between nodes placed in inner and outer faces where splitting cracks appear (Burgers et al., 2007)(see Figure 17b).

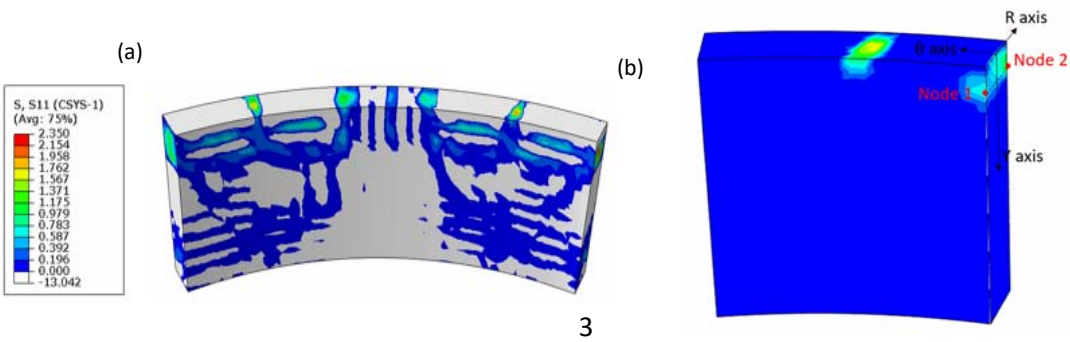

Figure 17 – Segment deformed shape for P_{sp} (a) Radial tensile stresses (b) Radial plastic strain and crack measurement scheme.

The P/P_{sp} - w_{sp} curves are represented in Figure 18. The maximum w_{sp} numerically detected for P_{acc} is lower than 0.05 mm and no significant differences are noticed between FRC strength classes. Hence, the spalling cracks appear to be those governing the post-cracking tensile strength requirements.

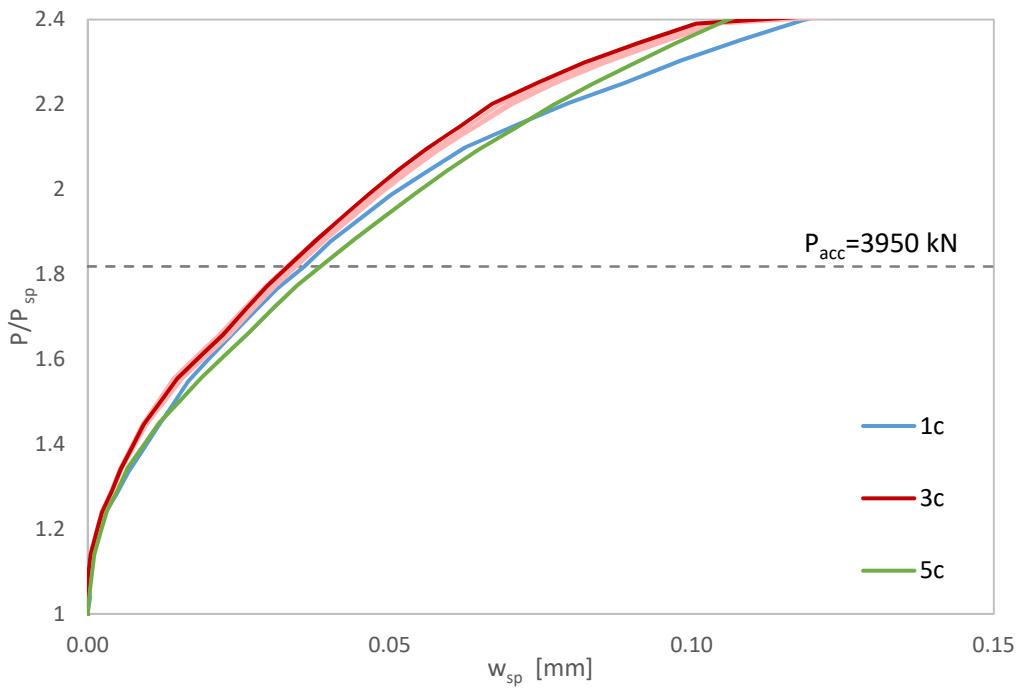

Figure 18 – Non-dimensional load – splitting crack opening

5.2. Eccentric thrust

Thrust has been simulated by considering an eccentricity (e) of 30 mm inwards (e=-30 mm) and outwards (e=+30mm) as Figure 19 shows. Both spalling and splitting cracks have been compared to centred thrust situation. Figure 20 depicts the relation of $P_{cr}/P_{spall,e=0}$ with the eccentricity for FRC.

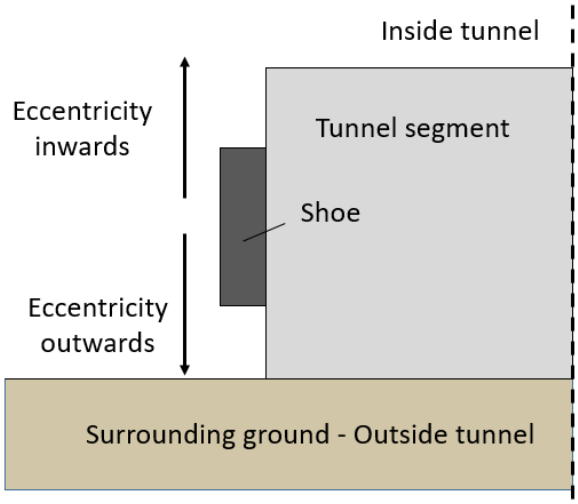

Figure 19 –Side view tunnel segment. Eccentricity scheme.

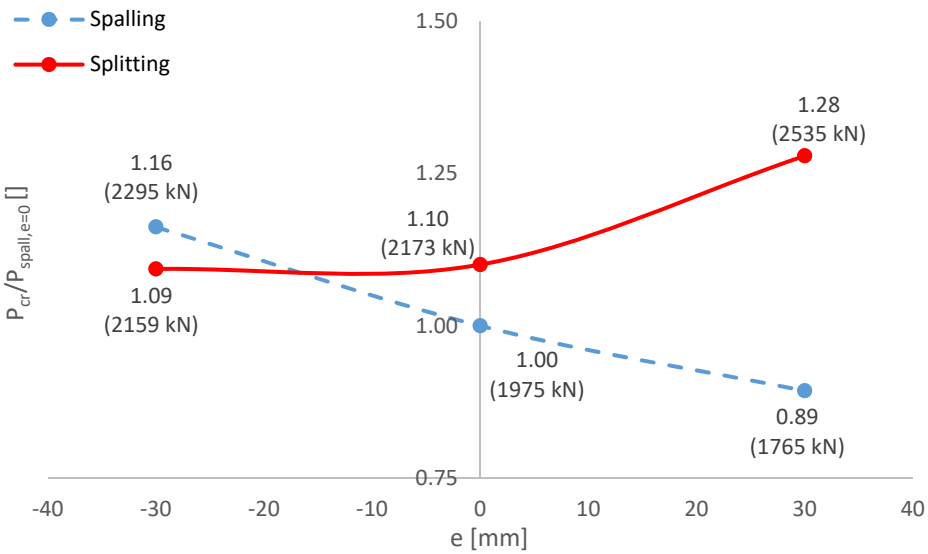

Figure 20 –Cracking load/spalling cracking load for e = 0 – eccentricity relationship for FRC.

As it occurred for centred loading ($P_{spall,e=0}$ = 1975 kN), according to Figure 20, for e > 0 the first crack is due to spalling stresses ($P_{spall}/P_{spall,e=0}$ = 0.89; e = +30 mm) and the second is due to splitting ($P_{sp}/P_{sp,e=0}$ = 1.28; e = 30 mm), whilst for e < 0 the crack appears firstly due to splitting stresses ($P_{sp}/P_{sp,e=0}$ = 1.09; e = -30 mm) followed by a spalling crack ($P_{spall}/P_{spall,e=0}$ = 1.16; e = -30 mm). It must be noticed that for e < 0 the cracking resistance increases respect to the centred thrust; this, nonetheless, must be taken with precaution since the existence of the gasket could slightly modify these results.

Figure 21 gathers $P/P_{spall,e=0}$ – spalling crack width relationship for the different values of the eccentricity analysed. Likewise, Table 3 gathers the P_{spall} loads and the spalling crack widths for P_{acc} ($w_{spall,acc}$) compared to those obtained for the centred thrust ($P_{spall,e=0}$ and $w_{spall,acc,e=0}$, respectively).

According to the results presented in Figure 21, it is remarkable that higher FRC strength classes have the ability to reduce the eccentricity effect on the crack openings. For instance, the 5c FRC class has a $w_{spall,acc}/w_{spall,acc,e=0}$ ratio of 1.06 and 1.00 for both e=+30mm and e=-30mm, which means that the effect of the eccentricity is controlled due to the great tensile residual strength of the FRC. Contrarily, the effect of eccentricity on the crack width is less effective as the FRC class is reduced.

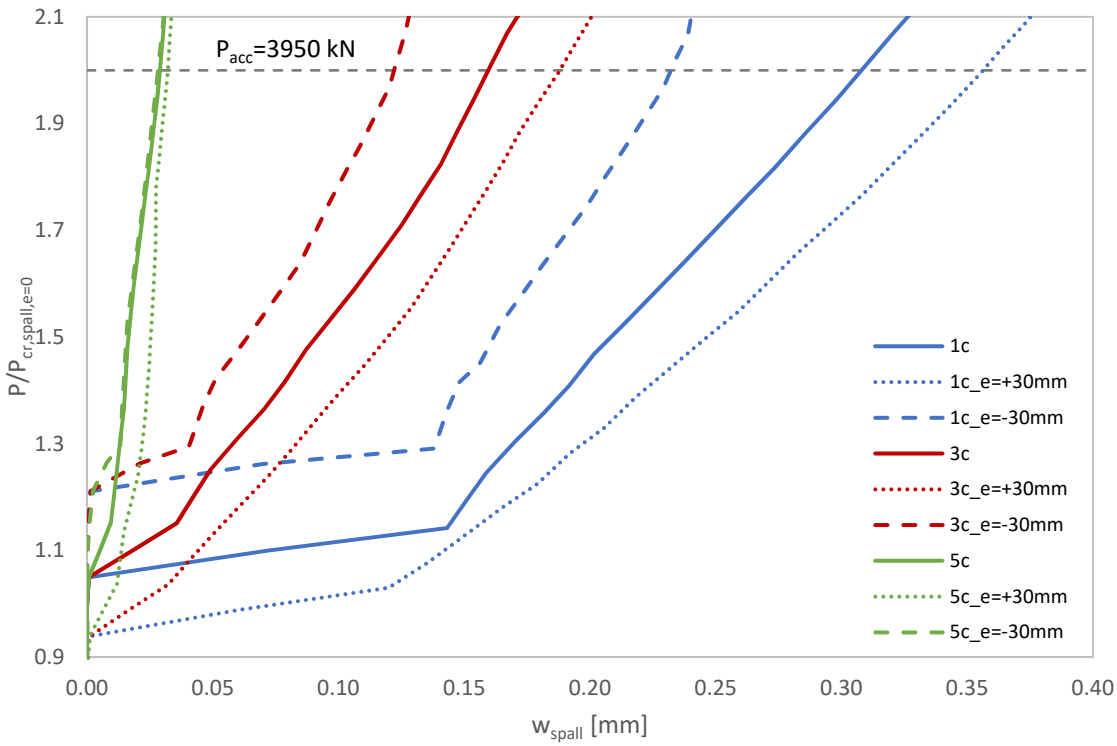

Figure 21 – Load/spalling cracking load for e = 0 – spalling crack width relationship

		P_{spall} [kN]	$P_{spall}/P_{spall,e=0}$	$w_{spall,acc}$ [mm]	$w_{spall,acc}/w_{spall,acc,e=0}$
e=+30 mm	PC	1765	0.89	0.43	1.13
	1c			0.35	1.16
	3c			0.18	1.12
	5c			0.04	1.06
e=-30 mm	PC	2160	1.09	0.28	0.73
	1c			0.23	0.76
	3c			0.12	0.75
	5c			0.03	1.00

Table 3 – Spalling cracking Load and maximum crack width for eccentric loading

Based on the results presented in Figure 21 and Table 3, it can be noticed that as the FRC strength class increases the spalling crack width is reduced drastically. The 3c FRC (see Figure 22) results to be the most suitable for controlling the crack width (while optimizing the amount of fibres) since the crack widths ranges between 0.12 mm (e = -30 mm) and 0.18 mm (e =+ 30 mm), which is an acceptable range (w < 0.20 mm)

for dealing with the posterior service conditions; this considering that the probability of reaching P_{acc} must be, by definition, very low.

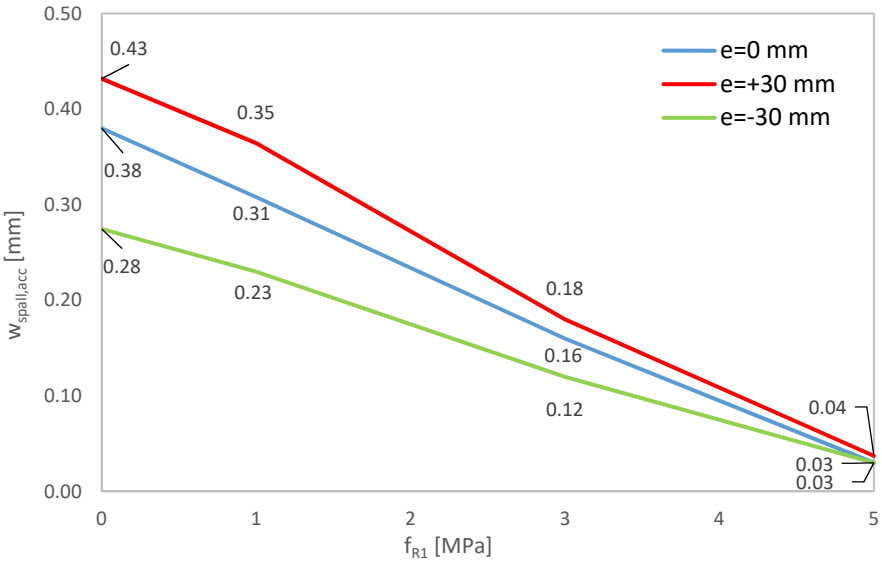

Figure 22 – Relation between f_{R1k} and $w_{spall,acc}$ for P_{acc} considering different eccentricities

Table 4 gathers the P_{sp} loads and the splitting crack widths for P_{acc} ($w_{sp,acc}$) compared to those obtained for the centred thrust ($P_{sp,e=0}$ and $w_{sp,acc,e=0}$, respectively). Figure 20 shows the non-dimensional $P/P_{sp,e=0} - w_{sp}$ relationship for the different values of the eccentricity considered.

The results shown in both Figure 23 and Table 4 reveal that eccentric thrust has a relevant influence on splitting cracks width whilst the FRC strength class influence barely affects the response (except for the 5c FRC and e=-30mm, which allows a better control of $w_{sp,acc}$). In this regard, $w_{sp,acc}$ increases up to 3.3 and 6.0 times $w_{sp,acc,e=0}$, for e=+30mm and e=-30mm respectively. Although $P_{sp,e=+30}$ is higher than $P_{sp,e=0}$, the former reaches higher values of crack width. For e<0, the splitting crack is produced at the same load level ($P_{sp,e=-30}/P_{sp,e=0}$ = 1.00); however, e>0 thrust lead to a greater crack growth in comparison to centred thrust.

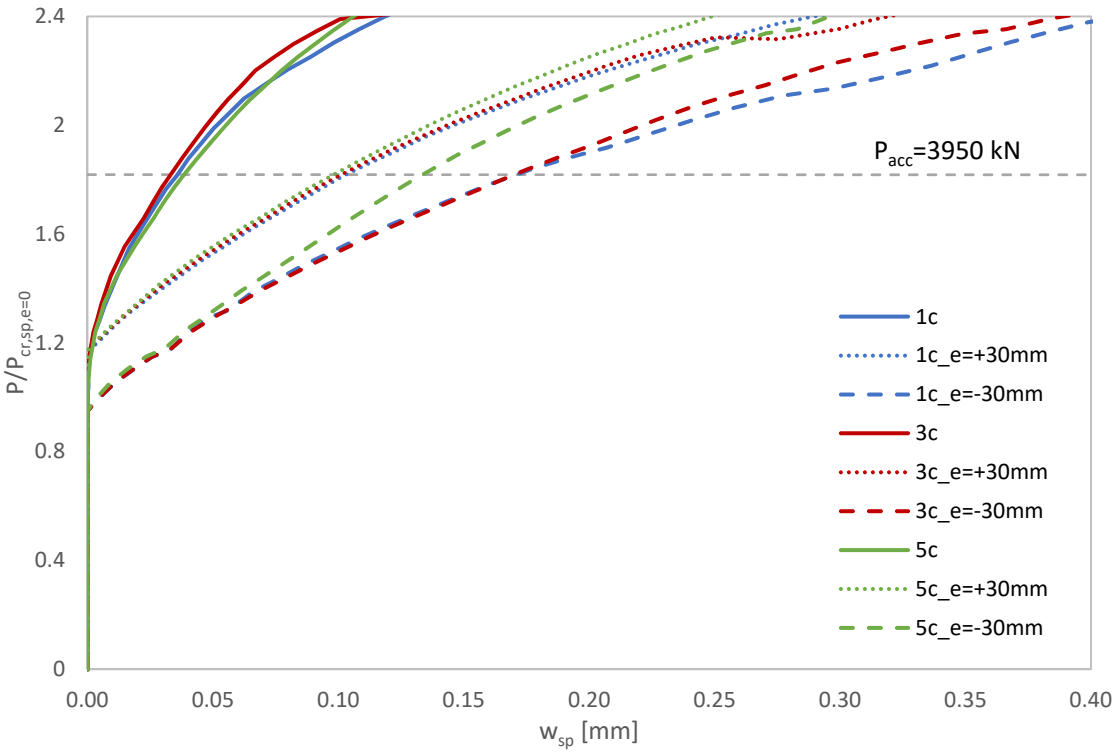

Figure 23 – Non-dimensional load – splitting crack opening for different eccentricities

		P_{sp} [kN]	$P_{sp}/P_{sp,e=0}$	$w_{sp,acc}$ [mm]	$w_{sp,acc}/w_{sp,acc,e=0}$
e=+30mm	Plain	2535	1.16	0.10	3.33
	1c			0.10	3.33
	3c			0.10	3.33
	5c			0.10	3.33
e=-30mm	Plain	2159	1.00	0.18	6.00
	1c			0.18	6.00
	3c			0.18	6.00
	5c			0.13	4.33

Table 4 – Splitting cracking load and maximum crack width for eccentric loading

5.3. Hybrid reinforced segment

Spalling cracks have proven to be the most concerning (wider) cracks during thrust phase for this segment geometry and thrust transfer configuration. In order to reduce these cracks while maintaining a competitive reinforcement configuration from both economical and time-saving perspectives, hybrid reinforcement (R/FRC) can be an optimal solution. Segments cast with plain, 1c, 3c and 5c FRC classes combined with two rebar configurations $\rho_{s,min}$ and $\rho_{s,min}/2$ (see Figure 9) are simulated with centred and eccentric thrust (e=±30mm).

Figure 25 gathers the spalling crack loads of hybrid configurations for centred and e=±30mm. The R/FRC solutions are able to increase P_{spall} compared to FRC in the centred configuration (2067 kN), in case of e=+30mm the cracking load for hybrid solution with $\rho_{s,min}$ (FRC+ $\rho_{s,min}$) is less affected by the eccentric thrust

than the other solutions. Regarding to e < 0, it is worth noticing that the cracking load remains the same for hybrid solutions respect to the centred thrust and, as aforementioned, must be taken with precaution since the existence of the gasket could slightly modify these results.

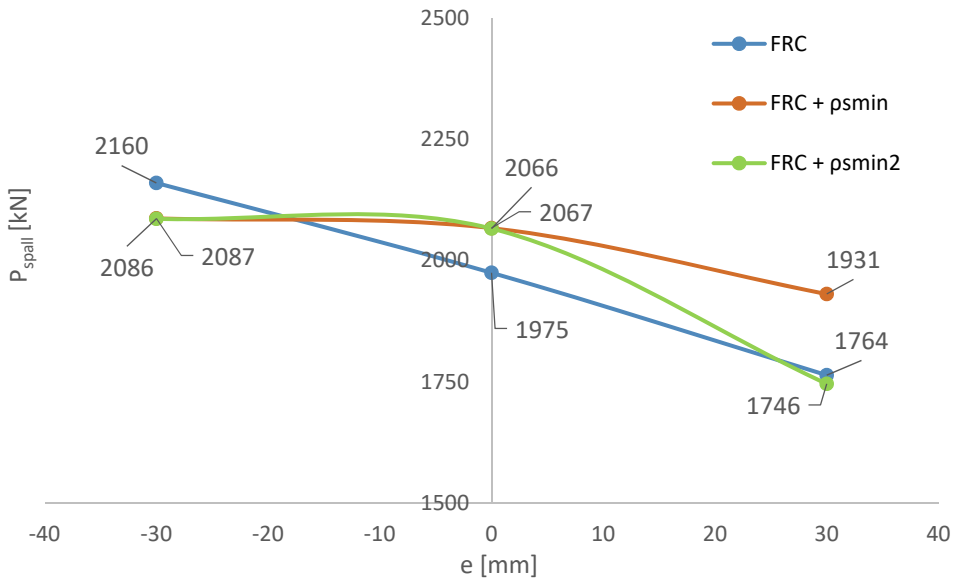

Figure 25 – Spalling cracking load for FRC and R/FRC segments for different eccentricities

Figure 26 depicts the $P/P_{spall,e=0} - w_{spall}$ relationship for centred thrust for all types of FRC. It can be noticed that the hybrid reinforcement is able to control better the crack width if this is compared to the FRC configuration for all reinforcement and eccentricity configurations; particularly. Figure 27 present the spalling crack width for P_{acc} for the whole range of eccentricities. As for the results presented in Figure 16, the spalling crack opening is based on the assumption that only one crack occurs in the spalling cracked regions and measured as the tangential relative separation between two adjacent nodes. In this sense, in case of hybrid reinforcement the assumption is conservative since multiple cracks are expected as a result of the collaboration between fibres and rebars.

The results of Figure 26 allow confirming that the rebar reinforcement has impact in reducing the crack width for low FRC strength classes (1c); contrarily, the rebar reinforcement has less efficiency for higher FRC strength classes (3c and 5c) since the crack width is already well-controlled ($w_{spall} \leq 0.20$ mm) by solely the fibre reinforcement (FRC). Nonetheless, the R/FRC solution for medium and high FRC strength classes is a suitable solution when either very strict crack width limitations are imposed (e.g., $w \leq 0.15$ mm) and/or when traditional steel reinforcement is also required to resist bending moments superior to the cracking bending moment (M_{cr}); for which, the FRC as unique reinforcement can be an uneconomical alternative (Liao et al., 2015a).

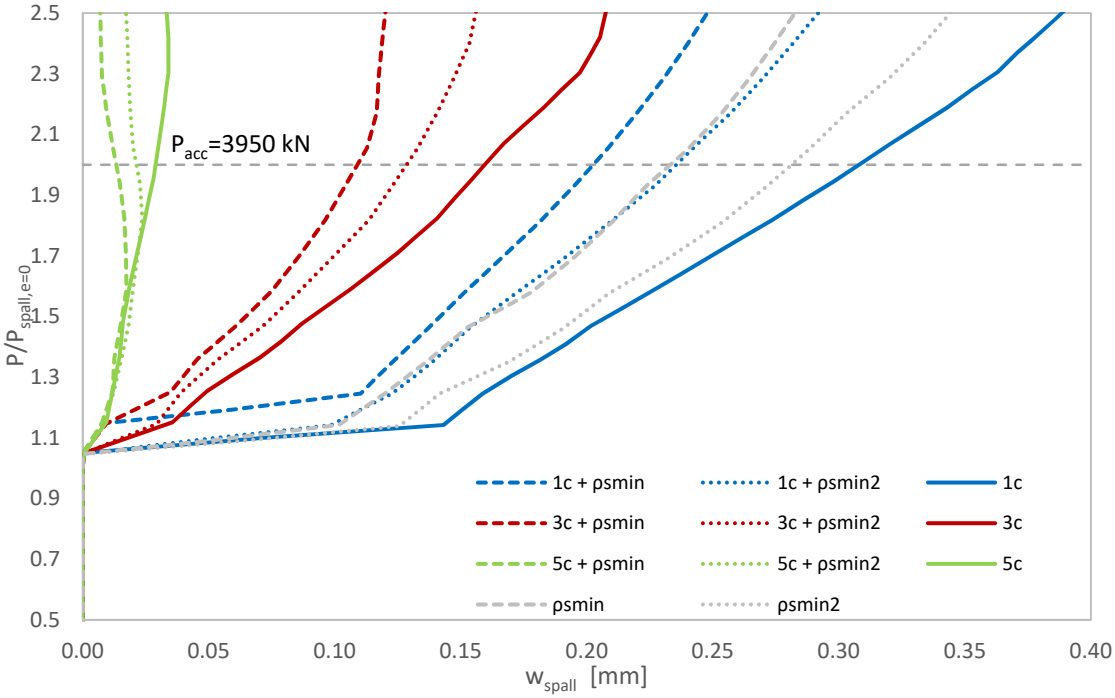

Figure 26 – Non-dimensional load – spalling crack opening for RC and R/FRC segments (for e = 0)

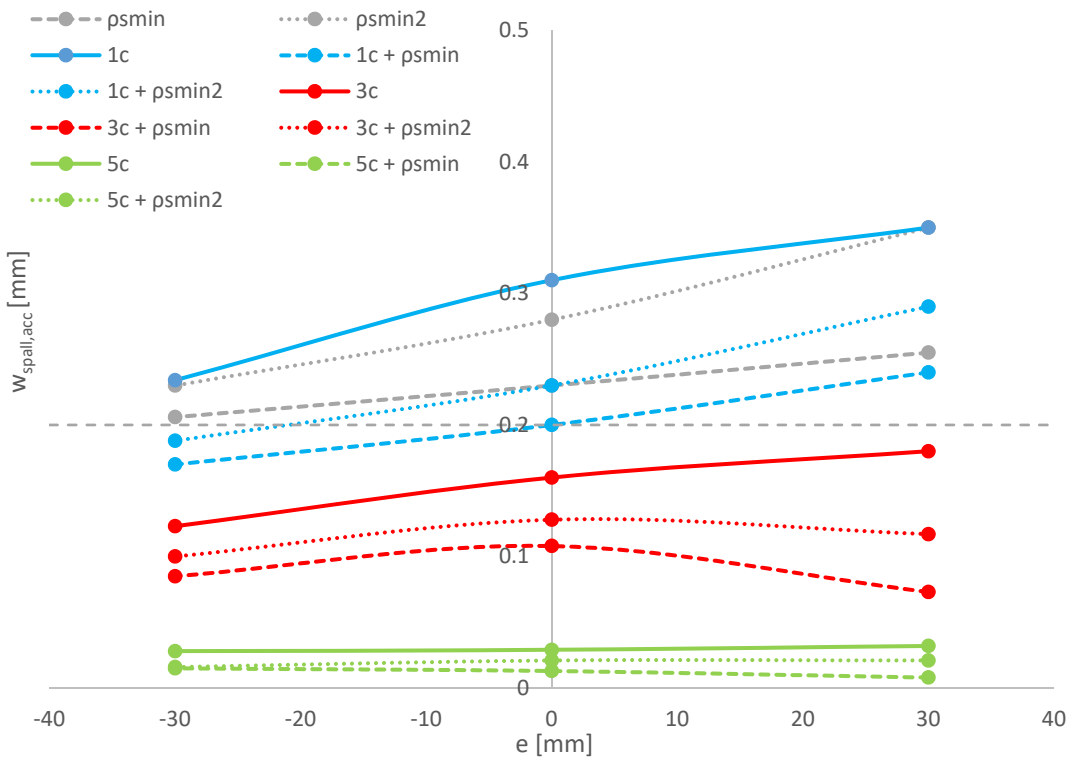

Figure 27 – Spalling crack opening – eccentricity for, 1c, 3c and 5c hybrid solutions

6. CONCLUSIONS

The thrust phase of TBM-bored tunnels supported with segmental linings considering different FRC strength classes and hybrid solutions (R/FRC) is investigated from a numerical point of view by means of a 3D non-linear FE model contrasted with experimental results. By using this model, spalling and splitting cracks for a range of thrust eccentricities are estimated and compared according to the different reinforcement configurations.

Based on a particular segment geometry and a thrust transfer configuration, the following conclusions can be drawn:

1. The residual flexural strength for a crack width of 0.5 mm (f_{R1}) has resulted to have a great influence in cracking control whilst the ratio f_{R3}/f_{R1} seems not play a significant role. This is of relevant importance when deciding the type of fibre (material and geometry) to be used since those that lead to higher f_{R1} would be more appropriate than those that perform better for larger crack widths.
2. The spalling cracks appear to be those governing the FRC post-cracking tensile strength requirements. Eccentric thrust has a relevant influence on cracking performance; in this sense, attention must be paid for both cracking phenomena, specially, for splitting cracks for which cracks up to 6.0 times wider respect to the perfectly centred thrust have registered.
3. Hybrid reinforcement leads to crack reduction and this can be considered as a suitable solution when severe crack width limitations are stablished for service.

It is worth noticing that the numerical simulations were carried out on a fixed segment geometry and bearing pads configuration; however, the abovementioned conclusions are also extendable to tunnels linings with other internal diameters and thicknesses and similar pads configurations considered.

Acknowledgements

The first author acknowledges the Spanish Ministry of Science, Innovation and University for providing support through the PhD Industrial Fellowship (DI-17-09390) in collaboration with Smart Engineering Ltd. (UPC's Spin-Off). This research has been possible due to the economic funds provided by the SAES project (BIA2016-78742-C2-1-R) of the Spanish Ministry of Economy, Industry and Competitiveness (MINECO).

REFERENCES

Abbas, S., Soliman, A., Nehdi, M., 2014. Structural behaviour of ultra-high performance fibre reinforced concrete tunnel lining segments. FRC 2014 Jt. ACI-fib Int. Work. Fibre Reinf. Concr. Appl. 532–543.

ACI 544.7R-16, 2016. Report on Design and Construction of Fiber-Reinforced Precast Concrete Tunnel Segments. ACI Comm. Rep. 1–36.

ACI 544, 2014. Fibre-Reinforced Concrete: Design and Construction of Steel Fibre- Reinforced Precast Concrete Tunnel Segments.

Beňo, J., Hilar, M., 2013. Steel fibre reinforced concrete for tunnel lining - Verification by extensive laboratory testing and numerical Modelling. Acta Polytech. 53, 329–337. https://doi.org/1049 [pii]

Blom, C.B.., 2002. Design philosophy of concrete linings in soft soils 70.

Breitenbücher, R., Meschke, G., Song, F., Hofman, M., Zhan, Y., 2014. Experimental and numerical study on the load-bearing behaviour of steel fibre reinforced concrete for precast tunnel lining segments under concentrated loads. FRC 2014 Jt. ACI-fib Int. Work. Fibre Reinf. Concr. Appl. 417–429.

Burgers, R., 2006. Non-linear FEM modelling of steel fibre reinforced concrete. Delft Univ.

Burgers, R., Walraven, J., Plizzari, G.A., Tiberti, G., 2007. Structural behaviour of SFRC tunnel segments during TBM operations 1461–1468.

Caratelli, A., Meda, A., Rinaldi, Z., 2012. Design according to MC2010 of a fibre-reinforced concrete tunnel in Monte Lirio, Panama. Struct. Concr. 13, 166–173. https://doi.org/10.1002/suco.201100034

Caratelli, A., Meda, A., Rinaldi, Z., Romualdi, P., 2011. Structural behaviour of precast tunnel segments in fiber reinforced concrete. Tunn. Undergr. Sp. Technol. 26, 284–291. https://doi.org/10.1016/j.tust.2010.10.003

Caratelli, A., Meda, A., Rinaldi, Z., Spagnuolo, S., 2016. Precast Concrete Tunnel Segments with GFRP Reinforcement. Tunn. Undergr. Sp. Technol. 60, 10–20. https://doi.org/10.1061/(asce)cc.1943-5614.0000803

Caratelli, A., Meda, A., Rinaldi, Z., Spagnuolo, S., Maddaluno, G., 2017. Optimization of GFRP reinforcement in precast segments for metro tunnel lining. Compos. Struct. https://doi.org/10.1016/j.compstruct.2017.08.083

Cavalaro, S., Blom, C.B.., Walraven, J., Aguado, A., 2012. Formation and accumulation of contact deficiencies in a tunnel segmented lining. Appl. Math. Model. 36(9), 4422–4438.

Cavalaro, S., Blom, C.B.., Walraven, J., Aguado, A., 2011. Structural analysis of contact deficiencies in segmented lining. Packer behaviour under simple and coupled stresses. Tunn. Undergr. Sp. Technol. 26, 734–749.

CEB-FIP, 2010. Model Code 2010. https://doi.org/10.1007/s13398-014-0173-7.2

Cervenka, V., Cervenka, J., Janda, Z., 2013. ATENA Program Documentation. Cerv. Consult.

CNR-DT 204/2006, 2007. Guide for the Design and Construction of Fibre-Reinforced Concrete Structures. Ital. Natl. Res. Counc. (CNR), Rome, Italy. 75. https://doi.org/10.14359/10516

Conforti, A., Tiberti, G., Plizzari, G., 2016a. Combined effect of high concentrated loads exerted by TBM hydraulic jacks. Mag. Concr. Res. 68, 1122–1132. https://doi.org/10.1680/jmacr.15.00430

Conforti, A., Tiberti, G., Plizzari, G., Caratelli, A., Meda, A., 2016b. Precast tunnel segments reinforced by macro-synthetic fibers. Tunn. Undergr. Sp. Technol. 63, 1–11. https://doi.org/10.1016/j.tust.2016.12.005

Conforti, A., Trabucchi, I., Tiberti, G., Plizzari, G.A., Caratelli, A., Meda, A., 2019. Precast tunnel segments for metro tunnel lining: A hybrid reinforcement solution using macro-synthetic fibers. Eng. Struct. 199, 149–296. https://doi.org/10.1016/j.engstruct.2019.109628

Dassault systems Simulia, C., 2012. Abaqus Analysis user's manual 6.12-3 1137.

de la Fuente, A., Blanco, A., Armengou, J., Aguado, A., 2017. Sustainability based-approach to determine the concrete type and reinforcement configuration of TBM tunnels linings. Case study: Extension line to Barcelona Airport T1. Tunn. Undergr. Sp. Technol. 61, 179–188. https://doi.org/10.1016/j.tust.2016.10.008

de la Fuente, A., Blanco, A., Pujadas, P., Aguado, A., 2015. Diseño óptimo de dovelas de hormigón

reforzado con fibras para el revestimiento de túneles. Hormigón y Acero 65, 267–279. https://doi.org/10.1016/j.hya.2014.11.002

de la Fuente, A., Pujadas, P., Blanco, A., Aguado, A., 2012. Experiences in Barcelona with the use of fibres in segmental linings. Tunn. Undergr. Sp. Technol. 27, 60–71. https://doi.org/10.1016/j.tust.2011.07.001

de Rivaz, B., Meda, A., Perruzza, P., Rinaldi, Z., Roumaldi, P., 2009. Full scale tests on precast tunnel segment made in concrete reinforced with high strength steel fibres.

de Waal, R.G.A., 2000. Steel fibres reinforced tunnel segments for the application in shield driven tunnel linings. Technische Universiteit Delft.

di Prisco, M., Plizzari, G., Vandewalle, L., 2009. Fibre reinforced concrete : new design perspectives. Mater. Struct. 1261–1281. https://doi.org/10.1617/s11527-009-9529-4

di Prisco, M., Toniolo, G., 2000. Structural applications of steel fibre reinforced concrete. Proc. Int. Work. Milan, Italy.

Dupont, D., Vandewalle, L., Erdem, E., Hemmy, O., Schnütgen, B., Steffen, S.H., 2001. Sub-task 4.4 - Splitting of SFRC induced by local forces 1–12.

EHE-08, 2008. Instrucción de Hormigón Estructrural (EHE-08).

European Commitee for Standardization, 2005. Precast concrete products - test method for metallic fibre concrete- Measuring the flexural tensile strength. Br. Stand. Inst. https://doi.org/9780580610523

FIB Bulletin 83, 2017. Precast Tunnel Segments in Fibre-Reinforced Concrete.

Gettu, R., Ramos, G., Aguado, A., García, T., Barragán, B., 2004. Steel Fiber Reinforced Concrete for the Barcelona Metro Line 9 Tunnel Lining. BEFIB 2004, Proc 6th RILEM Symp. FRC RILEM Symp, 1–46.

Hemmy, O., 2001. Sub-task 4.4 - Splitting of SFRC induced by local forces - Annex C Investigation of tunnel segments without curvature 1–32.

Hilar, M., Vítek, J., Pukl, R., 2012. Load testing and numerical modelling of SFRC segments 1–10.

Iyengar, K., 1962. Two-dimensional theories in anchorage zone stresses in Post- Tensioned prestressed beams. Heron 32, 45–56.

Jamshidi, M., Hoseini, A., Vahdani, S., de la Fuente, A., 2018a. Numerical-aided design of fiber reinforced concrete tunnel segment joints subjected to seismic loads. Constr. Build. Matreials 170, 40–54.

Jamshidi, M., Hoseini, A., Vahdani, S., de Santos, C., de la Fuente, A., 2018b. Seismic fragility curves for vulnerability assessment of steel fiber reinforced concrete segmental tunnel linings. Tunn. Undergr. Sp. Technol. 78, 259–274. https://doi.org/10.1016/j.tust.2018.04.032

Leonhardt, F., Mönnig, E., 1973. Berlin: Springer-Verlag; 1973 (Italian version: Leonhardt F, Mönnig E (1986) Casi speciali di dimensionamento nlle costruzioni in c.a. e c.a.p., vol. 2, Edizioni di Scienza e Tecnica, Milano). Tailor Made Concr. Struct. 66–66. https://doi.org/10.1201/9781439828410.ch37

Liao, L., de la Fuente, A., Cavalaro, S., Aguado, A., 2016. Design procedure and experimental study on fibre reinforced concrete segmental rings for vertical shafts. Mater. Des. 92, 590–601. https://doi.org/10.1016/j.matdes.2015.12.061

Liao, L., de la Fuente, A., Cavalaro, S., Aguado, A., 2015a. Design of FRC tunnel segments considering the ductility requirements of the fib Model Code 2010: Application to the Barcelona Metro line 9. Tunn. Undergr. Sp. Technol. 47, 200–210.

Liao, L., de la Fuente, A., Cavalaro, S., Aguado, A., Carbonari, G., 2015b. Experimental and analytical study of concrete blocks subjected to concentrated loads with an application to TBM-constructed

tunnels. Tunn. Undergr. Sp. Technol. 49, 295–306. https://doi.org/10.1016/j.tust.2015.04.020

Manie, J., Kikstra, W.P., 2008. Analusis procedures DIANA - Finite Element Analysis. User's Manual.

Meda, A., Rinaldi, Z., Caratelli, A., Cignitti, F., 2016. Experimental investigation on precast tunnel segments under TBM thrust action. Eng. Struct. 119, 174–185. https://doi.org/10.1016/j.engstruct.2016.03.049

Meda, A., Rinaldi, Z., Spagnuolo, S., de Rivaz, B., 2018. Precast concrete tunnel segments with GFRP reinforcement. ACI-fib-RILEM Int. Work.

MSC Software Corporation, 2008. MSC-Marc Manual.

NBN-B-15-238:1992, 1992. Essai des betons renforces des fibres. Essai de Flexion sur eprouvettes prismatiques (Testing of fiber reinforced concrete. Bending test on prismatic specimens) . Belgian Code - In French.

Plizzari, G.A., Tiberti, G., 2006. Steel fibers as reinforcement for precast tunnel segments. Tunn. Undergr. Sp. Technol. 21, 438–439. https://doi.org/10.1016/j.tust.2005.12.079

Pohn, J., Tan, K.H., Peterson, G.L., Wen, D., 2009. Structural testing of steel fibre reinforced concrete (SFRC) tunnel lining segments in Singapore. WTC 2009, Budapest, Hungary.

RILEM TC 162-TDF, 2003. Test and design methods for steel fibre reinforced concrete. Design with σ-ε method. Mater. Struct. 35, 262–278. https://doi.org/10.1617/13837

Schnütgen, B., Erdem, E., 2001. Sub-task 4.4 - Splitting of SFRC induced by local forces - Annex A.

Slenders, B.M.A., 2002. Modellering can boortunels (Dutch). Delft University of Technology and Projectorganisatie HSL-Zuid.

Sorelli, L.G., Toutlemonde, F., 2005. On the Design of Steel Fibre Reinforced Concrete Tunnel Lining Segments. 11th Int. Conf. Fract. 3–8.

Spagnuolo, S., Meda, A., Rinaldi, Z., Nanni, A., 2017. Precast concrete tunnel segments with GFRP reinforcement, Journal of Composites for Construction. https://doi.org/10.1590/1679-78251783

Sugimoto, M., 2006. Causes of Shield Segment Damages During Construction. Int. Symp. Undergr. Excav. Tunn. 67–74.

Swanson Analysis Systems, 2013. ANSYS User Manual.

Tiberti, G., 2004. Conci prefabbricati in calcestruzzo fibrorinforzato per la realizzazione di gallerie. Università degli studi di Brescia.

Tiberti, G., Conforti, A., Plizzari, G.A., 2015. Precast segments under TBM hydraulic jacks: Experimental investigation on the local splitting behavior. Tunn. Undergr. Sp. Technol. 50, 438–450. https://doi.org/10.1016/j.tust.2015.08.013

Tiberti, G., Plizzari, G.A., Walraven, J.C., Blom, C.B.M., 2008. Concrete Tunnel Segments with Combined Traditional and Fibre Reinforcement. Tailor Made Concr. Struct. Solut. Our Soc. (FIB Symp. 605–610. https://doi.org/10.1201/9781439828410.ch37